Intercomparison of Ground-Based Velocity Track Display (GBVTD)-Retrieved Circulation Centers and Structures of Hurricane Danny (1997) from Two Coastal WSR-88Ds

SHIRLEY T. MURILLO

NOAA/AOML/Hurricane Research Division, Miami, Florida

WEN-CHAU LEE AND MICHAEL M. BELL

UCAR/NCAR/EOL, Boulder, Colorado

GARY M. BARNES

University of Hawaii at Manoa, Honolulu, Hawaii

FRANK D. MARKS JR. AND PETER P. DODGE

NOAA/AOML/Hurricane Research Division, Miami, Florida

(Manuscript received 20 April 2009, in final form 29 April 2010)

ABSTRACT

A plausible primary circulation and circulation center of a tropical cyclone (TC) can be deduced from a coastal Doppler radar using the ground-based velocity track display (GBVTD) technique and the GBVTD-simplex algorithm. The quality of the retrieved primary circulation is highly sensitive to the accuracy of the circulation center that can only be estimated from the degree of scattering of all possible centers obtained in GBVTD-simplex analyses from a single radar in real TCs. This study extends previous work to examine the uncertainties in the GBVTD-simplex-derived circulation centers and the GBVTD-derived primary circulations in Hurricane Danny (1997) sampled simultaneously from two Doppler radars [Weather Surveillance Radar-1988 Dopplers (WSR-88Ds) in Mobile, Alabama, and Slidell, Louisiana] for 5 h.

It is found that the mean difference between the individually computed GBVTD-simplex-derived centers is 2.13 km, similar to the estimates in previous studies. This value can be improved to 1.59 km by imposing time continuity in the radius of maximum wind, maximum mean tangential wind, and the center position in successive volumes. These additional physical criteria, not considered in previous work, stabilized the GBVTD-simplex algorithm and paved the way for automating the center finding and wind retrieval procedures in the future.

Using the improved set of centers, Danny's axisymmetric tangential wind structures retrieved from each radar showed general agreement with systematic differences (up to 6 m s^{-1}) in certain periods. The consistency in the wavenumber-1 tangential winds was not as good as their axisymmetric counterparts. It is suspected that the systematic differences in the axisymmetric tangential winds were caused by the unresolved wavenumber-2 sine components rather than from the relatively small cross-beam mean wind components in Danny.

1. Introduction

Doppler radar has become the primary remote sensing instrument to deduce three-dimensional internal structures of tropical cyclones (TCs; e.g., Marks 2003). Wind damage and storm surge during a TC landfall are well correlated with the magnitude and areal extent of the primary circulation, which can be estimated using Doppler radial velocities at low levels. The structure and evolution of tropical cyclones have been studied with airborne pseudo-dual-Doppler radar for many years, primarily near the eyewall region (Marks and Houze 1984, 1987; Marks et al. 1992; Gamache et al. 1995). Physical insight into the storm structure and dynamics of TCs can be obtained through analyses of radar-derived kinematic fields

Corresponding author address: Shirley Murillo, NOAA/AOML/ Hurricane Research Division, 4301 Rickenbacker Causeway, Miami, FL 33149.
E-mail: shirley.murillo@noaa.gov

in Cartesian and cylindrical coordinates (Marks et al. 1992; Dodge et al. 1999; Reasor et al. 2000). However, because of the sampling limitations (flight duration and pattern) of airborne Doppler radar, previous studies were only able to document a snapshot of the TC evolution on a time scales of hours or days.

The Weather Surveillance Radar-1988 Doppler (WSR-88D) network in the United States and other countries (e.g., Taiwan, China, South Korea, and Japan) enables continuous monitoring of landfalling tropical cyclones within ~200 km of the coastline. These radars can sample a TC approximately every 6 min and reveal TC evolution with unprecedented time resolution (e.g., Blackwell 2000). However, the average distance between WSR-88Ds is ~250 km in the United States, thus making dual-Doppler analysis of the entire storm impractical and necessitates single-Doppler radar wind-retrieval techniques for deducing the TC circulation. It has been demonstrated that the primary circulation of a TC can be retrieved reasonably well from a single-Doppler radar using the ground-based velocity track display technique (GBVTD; Lee et al. 1999). The GBVTD technique has been used to study landfalling Typhoon Alex (1987) in Taiwan (Lee et al. 2000), Hurricane Charley (2004) in the United States (Lee and Bell 2007), and Typhoon Saomei (2006) in China (Zhao et al. 2008), revealing many features that had not been documented in previous Doppler radar observations. These authors all emphasized the importance of obtaining an accurate circulation center in order to accurately retrieve the TC circulation.

It has long been known that cylindrical coordinates provide a useful framework for studying vortex structure and dynamics. Within this conceptual framework the decomposition of a TC circulation into azimuthal wavenumber (harmonic) components has also proven to yield additional physical insights. For example, Willoughby (1992) demonstrated that a misplaced TC center resulted in an apparent wavenumber-1 asymmetry when decomposing an axisymmetric TC into azimuthal components. Since TCs are axisymmetric, the best TC center was defined as the point that minimizes the wavenumber-1 asymmetry. Marks et al. (1992) used a simplex method (Nelder and Mead 1965) to identify Hurricane Norbert's (1984) center from the pseudo-dual Doppler winds derived from observations of the National Oceanic and Atmospheric Administration (NOAA) WP-3D tail Doppler radar data. The circulation center was defined as a point that maximizes the storm-scale vorticity computed from a simplex method.

When the GBVTD-simplex algorithm was applied to Typhoon Alex (1987), Lee and Marks (2000, hereafter LM00) estimated the center accuracy was 1–2 km based on the scatter of multiple minima obtained through the simplex search. Alex's centers, obtained once every 15 min,

deviated from a straight line, similar to the trochoidal motion documented by Muramatsu (1986a), but with a smaller spatial and shorter temporal scale. With data available only from one Doppler radar in Typhoon Alex, it is not clear whether this motion was real or due to the uncertainty in the GBVTD-simplex algorithm. Without other independent measurements of the "true" TC center from reconnaissance aircraft and/or observations from another Doppler radar in Alex, it was not possible to assess the accuracy of the GBVTD-simplex TC center finding algorithm documented in their study. As the GBVTD algorithm becomes a primary tool for operation and research to diagnose TC structures using WSR-88D data, quantifying the uncertainties in the GBVTD-simplex-derived circulation centers and GBVTD-retrieved wind structure is necessary. Hurricane Danny (1997) provides a unique opportunity to examine the evolution of the wind and reflectivity fields of a TC that was simultaneously observed by two WSR-88Ds, Mobile, Alabama (KMOB), and Slidell, Louisiana (KLIX), from nearly perpendicular vantage points over 5 h. Hence, these two datasets can be considered independent and suitable to examine the uncertainties in the GBVTD-derived TC circulation and the GBVTD-simplex-derived TC circulation center.

The primary goals of the study are 1) to systematically compare these two independent sets (~60 volumes from each radar) of GBVTD and GBVTD-simplex solutions and to objectively evaluate the uncertainties in these algorithms, 2) to propose an improved TC center finding procedure by taking into account the time continuity of key TC characteristics, and 3) to solve for the full mean wind with data from both radars.

2. Analysis methods

a. The GBVTD technique

The GBVTD technique developed by Lee et al. (1999) is used to deduce the primary circulation of the storm using only single-Doppler radar observations. This technique is based on the principle that the TC circulation is nearly circular and can be represented spectrally in azimuthal space. With a known circulation center, the Doppler velocities at each radius can be Fourier decomposed into a series of sine and cosine functions. The 3D primary circulation of a TC can be reconstructed by compositing the primary circulation at each radius and height. The details of the GBVTD concept and technique are presented in Lee et al. (1999).

b. GBVTD-simplex center finding method

An accurate TC center is a prerequisite to retrieve accurate wind fields by the GBVTD technique (LM00). Although the axisymmetric circulation is less sensitive to
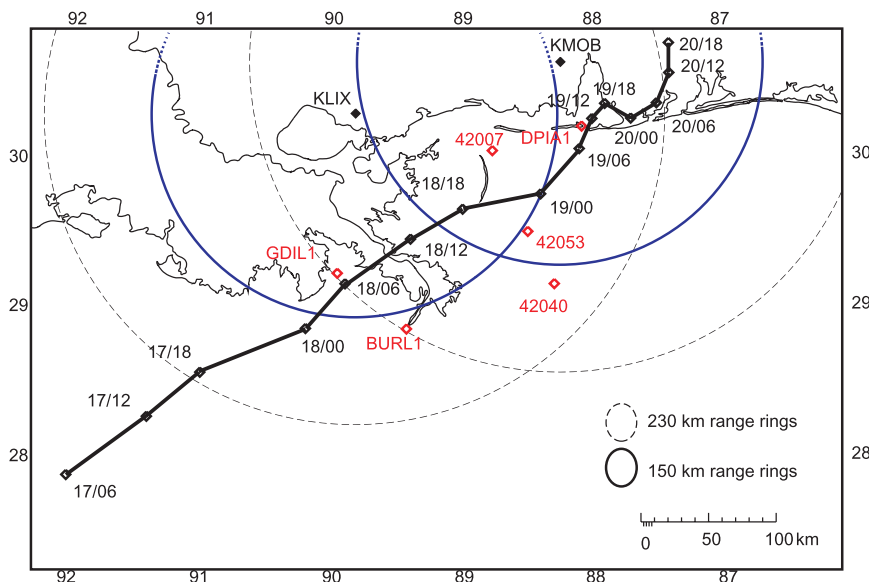
FIG. 1. Hurricane Danny (1997) best track plotted every 6 h. The open red diamonds show the location of the NOAA moored buoys and C-MAN platforms. WSR-88Ds KLIX and KMOB locations are each denoted with a black diamond and the 150 km (blue solid) and 230 km (black dashed) radar range rings are shown.

the uncertainty of the TC center, the TC center needs to be accurate within 5% of the radius of maximum wind (RMW) to keep the error in the retrieved asymmetric circulation below 20% (LM00). LM00 proposed the GBVTD-simplex center finding algorithm by incorporating the simplex method (Nelder and Mead 1965) into the GBVTD technique to provide an objective estimate of the TC center. The GBVTD-simplex method searches for a point that maximizes the mean tangential wind (e.g., wavenumber-0 component) of a tropical cyclone (Marks et al. 1992). Hence, both the RMW and the maximum mean tangential wind V_T can be estimated simultaneously. The GBVTD-simplex algorithm has been applied in several tropical cyclone studies (e.g., Lee et al. 2000; Lee and Bell 2007; Zhao et al. 2008).

Following the procedures outlined in LM00, we used 16 possible initial center positions surrounding the first-guess center location (estimated from reflectivity patterns or single-Doppler velocity patterns) for the GBVTD-simplex calculation. It is assumed that these initial center guesses will surround the "true center" and better identify "global" rather than "local" maximum mean tangential winds in the process. The use of 16 initial guesses was determined as a balance between computational efficiency and sufficient statistics to confidently determine a center. The separation (or the distribution) among these initial guesses is a function of the size of the eye and the uncertainty in estimating the initial center. The constant altitude plan position indicator (CAPPI) of reflectivity and Doppler velocity are made from PPI data using bilinear

interpolation (e.g., Mohr et al. 1986) then interpolated onto concentric rings in a cylindrical coordinates where its origin is the TC circulation center (Lee et al. 1999).

For each initial center, the calculations were performed on annuli with a width of 2 km centered on the estimated RMW of 20 km during the analysis period. Because of the inhomogeneous distribution of radar data above 5-km altitude, reliable centers could not be obtained there. The circulation above 5 km was retrieved using the center at 5 km. The estimated center location for each RMW is the arithmetic mean of center guesses from all 16 analyses. Estimated centers that are farther than one standard deviation from the estimated mean center for each apparent RMW and altitude are discarded and the TC center is recomputed by averaging the remaining points (LM00). The TC center and the RMW can then be selected at each altitude below 5 km based on the maximum mean tangential winds for each altitude.

c. Hurricane Danny (1997) and datasets

Hurricane Danny was a category-1 hurricane that made landfall at 0900 UTC 18 July 1997 near the mouth of the Mississippi River and again in the Mobile Bay area at 1000 UTC 19 July 1997 (Fig. 1). On 16 July 1997, an upper-level trough situated over the southeast United States set off a cluster of thunderstorms over the lower Mississippi valley. This convection drifted over the northern Gulf and contributed to the development of a weak surface low. Danny developed from this low in the northwest Gulf of Mexico and at 1200 UTC 16 July 1997

it was classified as a tropical depression. Peak winds reached 35 m s^{-1} with a minimum pressure of 984 hPa at 1500 UTC 19 July 1997. Danny stalled for about 15 h over Mobile Bay. It produced nearly 1000 mm of rain over the southern Alabama area (Rappaport 1999). Figure 2 shows the extent of the outer rainbands that produced heavy rainfall over the Bay depicted from the KLIX radar.

Danny moved east-northeast toward Mobile Bay along the Gulf coast before making landfall (Fig. 1). The storm was within the Doppler-velocity ranges of both KLIX and KMOB for 5 h. A U.S. Air Force Reserve WC-130 was performing a hurricane reconnaissance mission and a NOAA WP-3D was flying a landfall research mission during this period. GPS dropsondes were deployed throughout the storm from the aircraft. Several NOAA moored buoys and Coastal Marine Automated Network (C-MAN) platforms also were sampling the storm. For this study data from both KLIX and KMOB radars from 1600 to 2100 UTC 18 July 1997 were used.

d. WSR-88D data and data processing

This study uses WSR-88D archive level-II radar data from KLIX and KMOB. These data have the highest spatial resolution [1° beamwidth × 250 m along the beam length (range gate)] of all the archived data and are available in an unprocessed form (Crum et al. 1993). KLIX and KMOB level-II data were quality controlled (e.g., ground clutter removal, Doppler velocity unfolding, removing noise, and second-trip echoes) using the National Center for Atmospheric Research (NCAR) SOLO package (Oye et al. 1995) employing the Bargen and Brown (1980) Doppler velocity unfolding algorithm.

3. Improvements in TC center finding

a. Original GBVTD-simplex-derived centers

Danny's GBVTD-simplex-derived tracks from KLIX and KMOB data are shown in Fig. 3a. The mean, median, and standard deviation of the difference between these two sets of centers are illustrated in Table 1 (labeled as the ''original method''). Since the KLIX and KMOB scans were not coordinated to begin at the same time, the center locations were linearly interpolated into 1-min intervals to prevent differences due to staggered starting times of each radar volume. The RMW of Danny was approximately 18 km. The mean difference between these two sets of centers using the original method is ∼2.1 km, exceeding the 1.9-km threshold for an 18-km RMW recommended in LM00. The standard deviation of 1.2 km indicates that, assuming a normal distribution, there were more than 15% of the center pairs that differed more than one standard deviation (i.e., >3.3 km). Closer examination of the data in Figs. 3a,b reveals two apparent discrepancies.
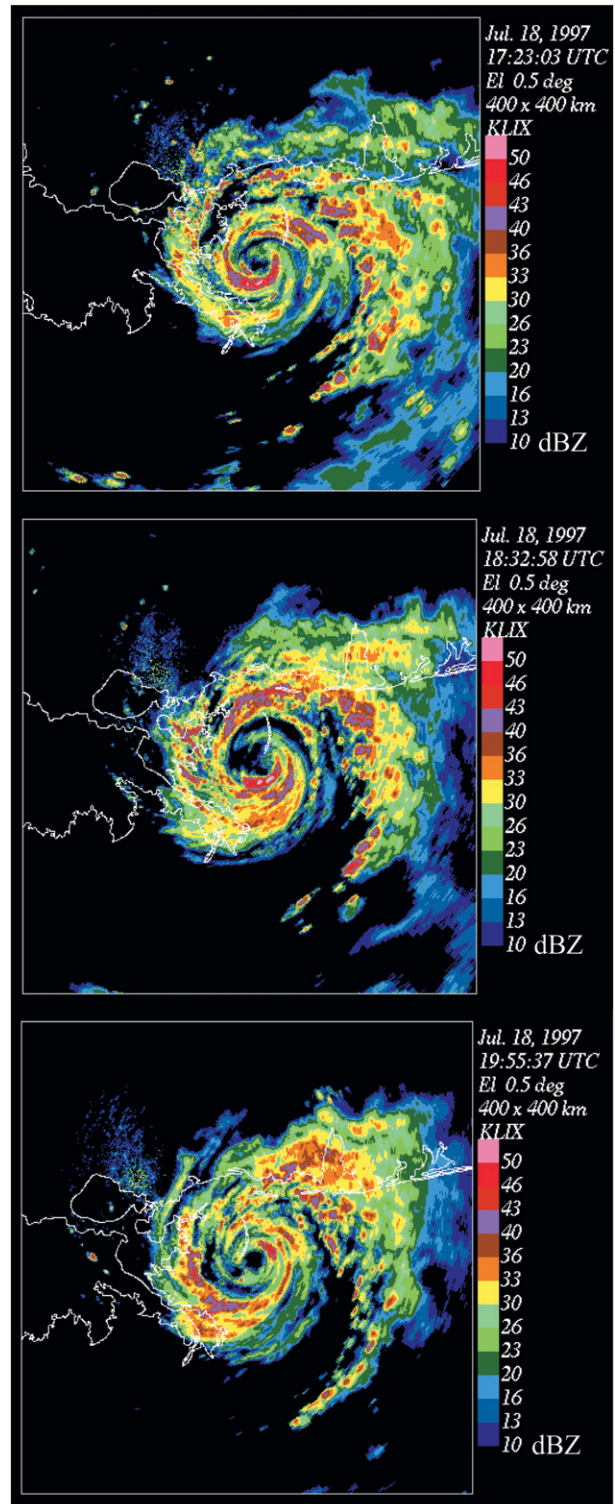

FIG. 2. KLIX base radar reflectivity images of Hurricane Danny approaching Mobile Bay, AL, at 1723, 1832, and 1955 UTC 18 Jul 1997.
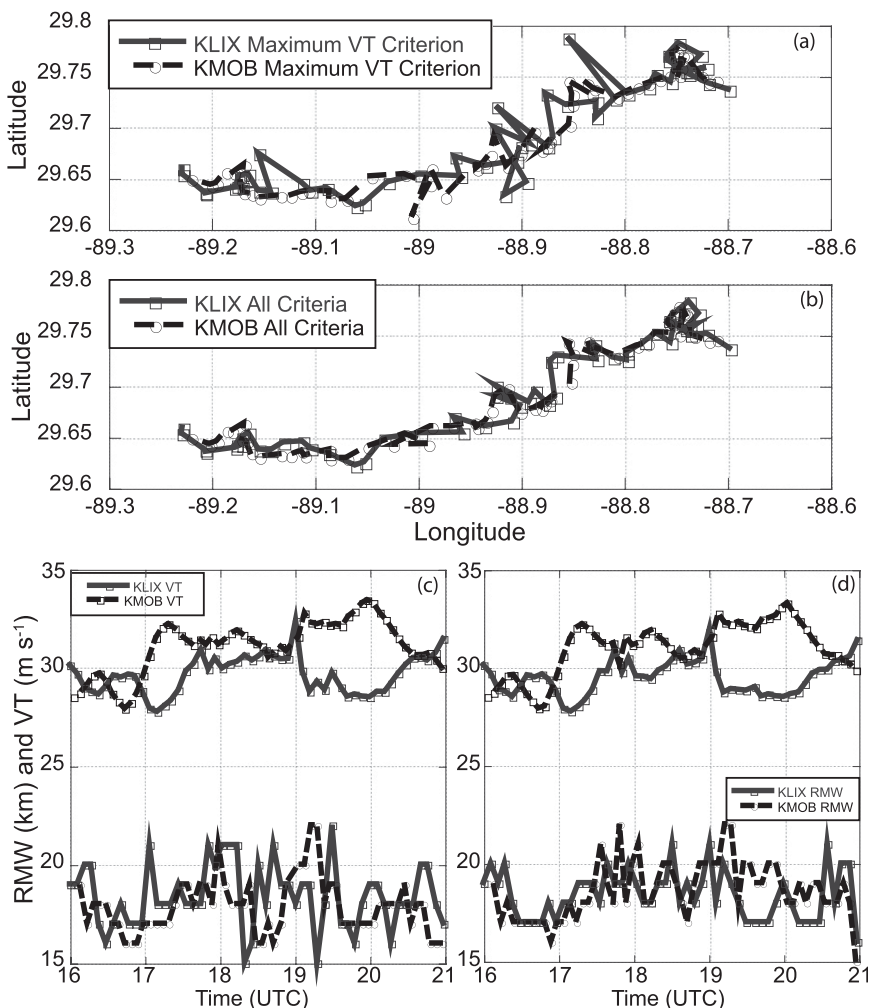
FIG. 3. (a) GBVTD-simplex centers at 2 km from KLIX and KMOB for Hurricane Danny using the original method that uses the maximum tangential wind as a criterion. (b) The GBVTD-simplex centers after applying the additional constraints discussed in the text. The GBVTD-derived mean tangential wind V_T at the RMW (c) using the original constraint and (d) using the additional constraints.

First, internal inconsistency on storm characteristics is apparent within each of the KMOB and KLIX analyses. Large fluctuations in derived quantities existed (sometimes from volume to volume) beyond the known uncertainties (e.g., ~2 km in center estimate and 1 km in RMW due to the width of the annulus). Examining the derived quantities from successive radar volumes revealed that the retrieved TC structures can be quite different when the GBVTD-simplex-derived centers differed more than several kilometers or the successive RMWs derived from the same radar deviated more than 2 km. Typically, an incorrect higher mean tangential wind value is deduced due to missing data at greater radii, the existence of an outer eyewall, and/or combinations of velocity dipoles at an incorrect RMW. In this situation, the derived center

may not be even close to the true center resulting in a completely different storm structure. Some of the fluctuations in TC center position in successive volumes appear to largely result from a relatively flat radial profile of the mean tangential wind speed near the RMW, such that the algorithm may choose different RMWs because of small perturbations in the derived mean tangential winds. Essentially, the original GBVTD-simplex algorithm has too many degrees of freedom in finding the maximum mean tangential wind without considering the physical integrity and time continuity of the TC structures; therefore, making the GBVTD-simplex algorithm very sensitive to inhomogeneous spatial data distribution.

Second, systematic differences in the retrieved TC quantities existed between these two independent

TABLE 1. Statistics on the differences between GBVTD-simplex-derived storm center estimates using the ''original'' method and the ''new'' method, which takes into account TC structure continuity.

Difference between TC center estimates for KLIX and KMOB		
	Original method (km)	Improved method (km)
Mean	2.12	1.59
Median	1.89	1.37
Std dev	1.24	0.95
RMS	2.46	1.86

analyses. For example, up to 5 m s^{-1} differences between the maximum mean tangential winds (Fig. 3c) are apparent between 1900 and 2030 UTC. This discrepancy might be rooted in different viewing angles between KLIX and KMOB resulting in different aliasing magnitudes into the mean tangential winds from the unresolved terms such as the cross-beam mean winds and the sine component of the wavenumber 2 (Lee et al. 1999). This point will be discussed in section 5.

b. Comparisons with other circulation centers

Figure 4 illustrates the derived GBVTD-simplex centers for both radars along with the centers from other independent estimates [i.e., National Hurricane Center (NHC) operational radar center fixes and aircraft flight-level fixes] for comparison. The storm is passing through the Chandeleur Islands off the coast of Louisiana. The GBVTD-simplex-derived tracks are in general agreement with centers derived by other sources; however, the GBVTD-simplex-derived tracks show more details as they are computed every 6 min. The GBVTD-simplex-derived centers were within 10 km of the aircraft fixes. The GBVTD centers from KMOB and KLIX are consistent not only with each other, but also with the aircraft fixes and the KLIX and KMOB NHC operational radar centers.

c. The improved GBVTD-simplex-derived TC centers

Based on the findings in section 2a, several procedures were examined to improve the GBVTD-simplex-derived TC centers and the recommended procedures are discussed, and the quality of the centers resulting from these procedures is examined in this section.

1) INCLUDE ASYMMETRY IN THE CURVE FIT

LM00 used only wavenumber 0 in the fitting of TC circulation to the observed Doppler velocities along a constant radius. Since Danny was an asymmetric TC, it is intended to examine the effects of including asymmetry in addition to wavenumber 0 in the GBVTD-simplex
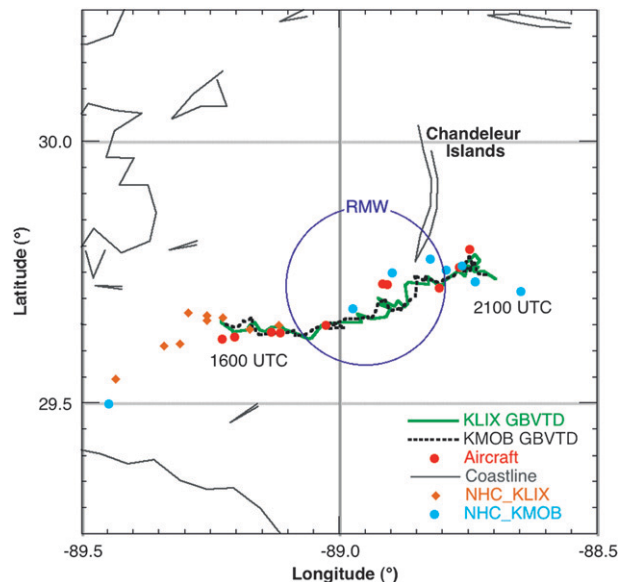

FIG. 4. Hurricane Danny's track as it crosses the Chandeleur Islands off the coast of Louisiana. Both GBVTD derived tracks are plotted as well as the aircraft and NHC operational radar fixes for comparison. The circle depicts the GBVTD-derived mean RMW for Danny (RMW = 18 km).

curve fit on the GBVTD-simplex algorithm. These results are illustrated in Fig. 5. The inclusion of wavenumber 1 (i.e., wave 0 + 1, see Fig. 5b) in the GBVTD-simplex algorithm reduced the variability in the center locations from the analyses only including wavenumber 0 (Fig. 5a). Including additional wavenumbers degraded the center estimates in this case (not shown).

It can be concluded that it is important to consider pronounced storm asymmetries in the GBVTD-simplex algorithm to yield the most consistent centers. This situation has been encountered in an elliptical-shaped Typhoon Herb (1996) with a significant wavenumber-2 asymmetry (Lee et al. 2002), whereas the GBVTD-simplex algorithm failed using only wavenumber 0 in the curve fit. The asymmetry of a TC can be inferred from the GBVTD analysis where an iterative procedure can be implemented based on the goodness of the curve fit to find the best fit (i.e., smallest overall standard deviation) to the observed Doppler velocities by including different wavenumbers.

2) IMPLEMENT CONSTRAINTS ON TC STRUCTURES IN SPACE AND TIME

The RMW, the maximum V_T, and the circulation center of a TC should evolve slowly and consistently in space and time without significantly large fluctuations during a 6-min period. These physical constraints should be applied when one selects the ''best center'' from the time series of the GBVTD-simplex-derived quantities within the uncertainties of the 1° beam resolution and
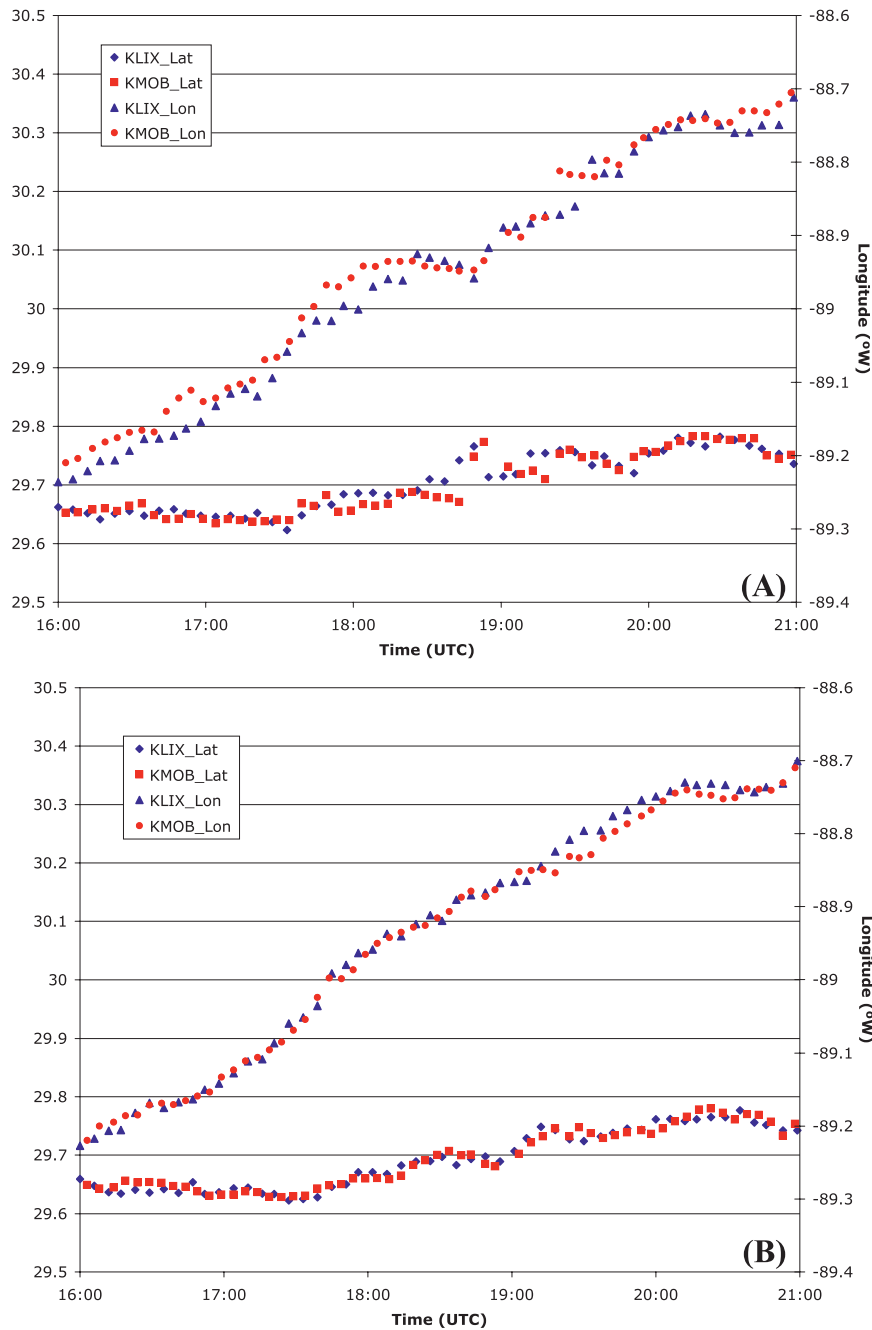
FIG. 5. GBVTD-derived storm positions at 2 km for KLIX and KMOB separated by storm position components (latitude and longitude) for (a) wavenumber 0 and (b) wavenumber 0 + 1.

the 1-km grid resolution. Based on these physical constraints, it is determined that the reasonable range of fluctuations for storm characteristics due to evolution and advection are 2 km for RMW, 5 m s^{-1} for maximum mean tangential wind, and 2 km for the circulation centers on consecutive radar volumes in this study.

Based on the above discussions, all possible GBVTD-simplex centers at each time during the 5-h were

reexamined and two new sets of centers were selected (Fig. 3b) and their corresponding RMWs and maximum mean tangential winds are illustrated in Fig. 3d. It is apparent that the unrealistic fluctuations in center position, RMWs and maximum V_T in the "original" algorithm (Figs. 3a,c) were drastically reduced in the "improved" algorithm (Figs. 3b,d). The consistency in these storm characteristics appeared not only in results from single
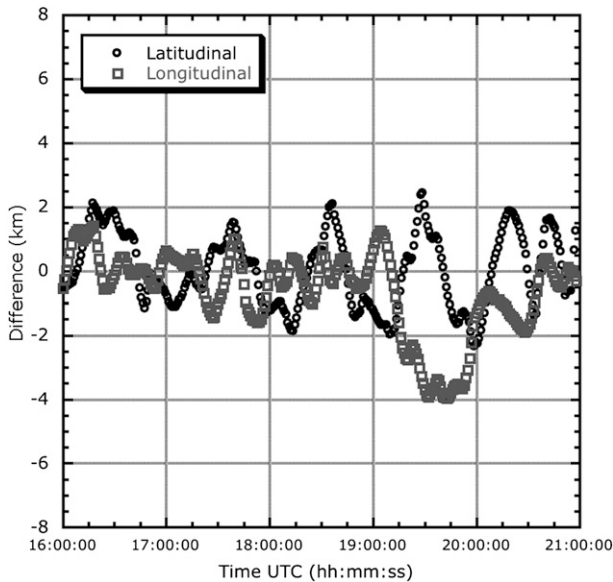
FIG. 6. Latitudinal (black circles) and longitudinal (gray squares) differences (km) for GBVTD-derived simplex center positions for KMOB and KLIX.

FIG. 7. Center differences (km) from each radar as well as differences with dual-Doppler observations.

radar (KLIX or KMOB) but also in the cross comparisons. The mean difference (standard deviation) between the center position obtained by KMOB and KLIX is reduced to 1.59 (0.95) km from 2.12 (1.24) km obtained in the original algorithm (Table 1). The large differences at the beginning and ending periods are a result of poor data coverage because Danny was either entering KMOB or leaving KLIX's Doppler ranges. The mean differences can be further reduced if these periods were excluded. Nevertheless, the mean center difference of 1.59 km resulting from two independent radar observations provides, for the first time, an objective assessment of the uncertainties in TC centers estimated by the GBVTD-simplex algorithm after taking into account the storm structures in the GBVTD-simplex algorithm.

Examining the differences in these two GBVTD-simplex centers (latitude and longitude) shown in Fig. 6 reveal temporal variability in both the latitude and longitude differences with magnitudes mostly less than 2 km except for the period between 1915 and 2045 UTC, where the largest difference is around 1930 UTC (>4 km). This period coincides with the out of phase characteristics seen in V_T (Fig. 3d), indicating a systematic bias in deducing the centers and TC structures. The majority of the RMW differences are within 1 km (the radius resolution of the cylindrical analysis grid) with the largest difference of 2–3 km once again occurring around 1930 UTC (Fig. 3). This period is consistent with the systematic differences shown in center locations (Fig. 6) and V_T (Fig. 3).
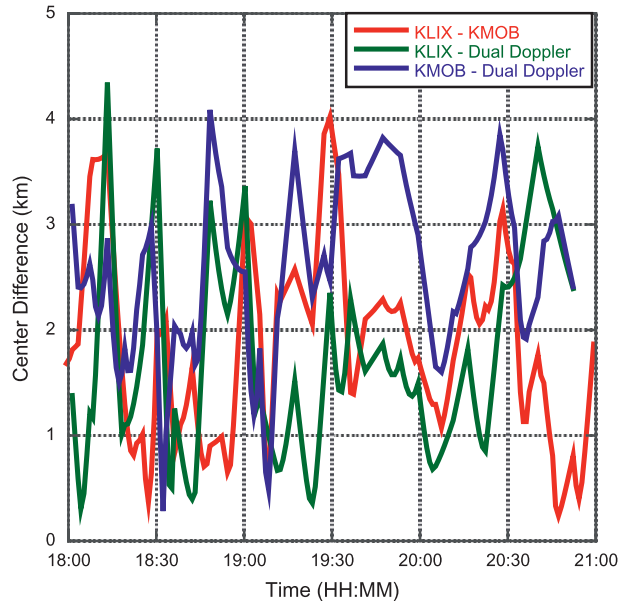
A comparison of the differences between the simplex-derived centers from each radar with the center differences with the dual-Doppler wind field (Fig. 7) was performed. The dual-Doppler center is obtained using the Marks et al. 1992 methodology, maximizing the vorticity at the RMW as in the GBVTD case, but using the full wind field. Additional physical constraints were not applied to the dual-Doppler centers though they are the center that maximizes the mean tangential wind from each combined radar volume independently. As can be seen from Fig. 7, neither KLIX or KMOB is doing significantly better than the other when compared to the dual Doppler, but they agree on average with the true center and with each other to within ~2 km. There is also no evident bias in the results, but mostly scatter.

4. Intercomparison of the GBVTD-derived TC structures

Using the improved set of Danny's centers, the kinematic structures of Hurricane Danny observed from both the KLIX and KMOB radars were deduced from the GBVTD technique for the entire 5 h with an unprecedented 6-min temporal resolution. Danny's kinematic structures (axisymmetric and wavenumber-1 reflectivity and tangential wind) are presented in time–radius space (Hovmöller diagram) and will be used to evaluate the quality of the GBVTD-retrieved TC structures during the storm's evolution.
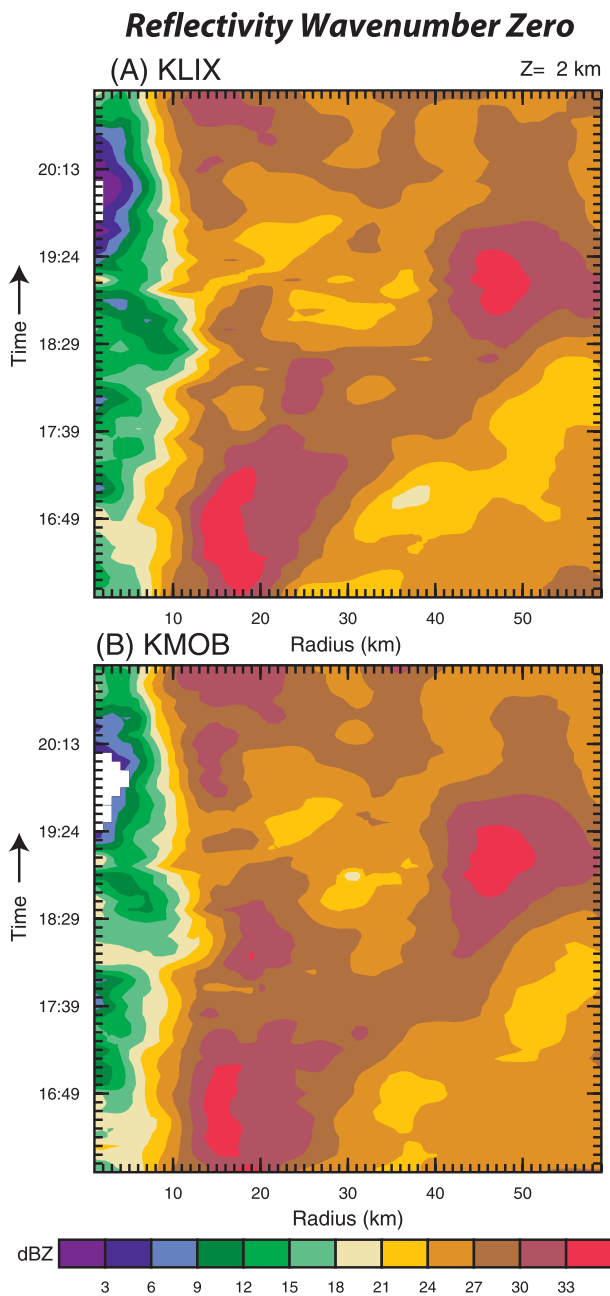
Reflectivity Wavenumber Zero

(A) KLIX

(B) KMOB

FIG. 8. Time–radius (Hovmöller) plot of Hurricane Danny reflectivity wavenumber 0 for (a) KLIX and (b) KMOB.

a. Reflectivity evolution

Hovmöller diagrams of the wavenumber 0 (axisymmetric mean) reflectivity at 2-km altitude for KLIX (Fig 8a) and KMOB (Fig. 8b) are shown. The reflectivity patterns from both radars are nearly identical, which is expected because reflectivity is a scalar. The similarity in Fig. 8 also indicates that the radar reflectivity is not biased between KLIX and KMOB. The radius of peak axisymmetric

reflectivity structure is located at $R \sim 18$ km with the maxima observed from both radars of ~33 dBZ between 1600 and 1700 UTC. The peak axisymmetric reflectivity weakened to ~30 dBZ between 1700 and 1900 UTC, while remaining at around 20-km radius. An outer reflectivity maximum located at $R \sim 47$ km began to intensify around 1700 and peaked around 1900 UTC. Afterward, the inner reflectivity maximum intensified and the radius contracted to ~14 km after 1900 UTC. Weaker reflectivity ($<$15 dBZ) persists inside the eyewall from $R = 0$–7 km.

The wavenumber-1 reflectivity patterns (Fig. 9) for both radars are also in good agreement. The length (direction) of the vector in Fig. 9 is proportional to the magnitude (phase, relative to the TC center) of the wavenumber-1 reflectivity. The large area of 14–22 dBZ, located 10–40 km southeast of the TC center from 1700 to 2000 UTC coincides with the minimum in the reflectivity wavenumber 0 (Fig. 8). This sequence of events suggests that Danny evolved from a nearly axisymmetric storm (before 1700 UTC) to an asymmetric wavenumber-1 storm then evolved back into an axisymmetric storm after 2000 UTC. The enhanced wavenumber-1 reflectivity in the southeast quadrant indicated a period with a convective burst from ~1700 to 1840 UTC. The location of the peak convection rotated cyclonically from south-southeast to east in this period ending at about 1930 UTC.

b. Kinematic evolution

Danny's axisymmetric wind structure is represented by wavenumber 0 at 2-km altitude (Fig. 10). The Hovmöller diagram for both KLIX (Fig. 10a) and KMOB (Fig. 10b) show the maximum tangential winds exceeding 30 m s^{-1} (also in Fig. 3d). The agreement between the KLIX and KMOB wavenumber 0 in Fig. 10 is definitely not as good as that in the wavenumber-0 reflectivity (Fig. 8). One should not be surprised at this discrepancy since V_T is a derived quantity that is dependent on the viewing angle in the GBVTD formulation. A steady increase of wavenumber-0 V_T is observed from KMOB with periodic episodes (duration ~1 h) of high wavenumber-0 V_T seen throughout the 5 h (Fig. 10b). A similar trend was also resolved in the KLIX analyses (Fig. 10a), but was not as clear as those shown in the KMOB analyses. KMOB analysis, in general, depicts stronger axisymmetric V_T than those resolved in KLIX, especially around the later periods (i.e., 2000 UTC). The differences between the two estimated axisymmetric V_Ts are typically within 2 m s^{-1} except for a short period near 1710 UTC and a long period between 1910 and 2030 UTC where the magnitudes of the differences reaches 4 m s^{-1}. The true axisymmetric V_T is probably in between these two estimates. Hence, the

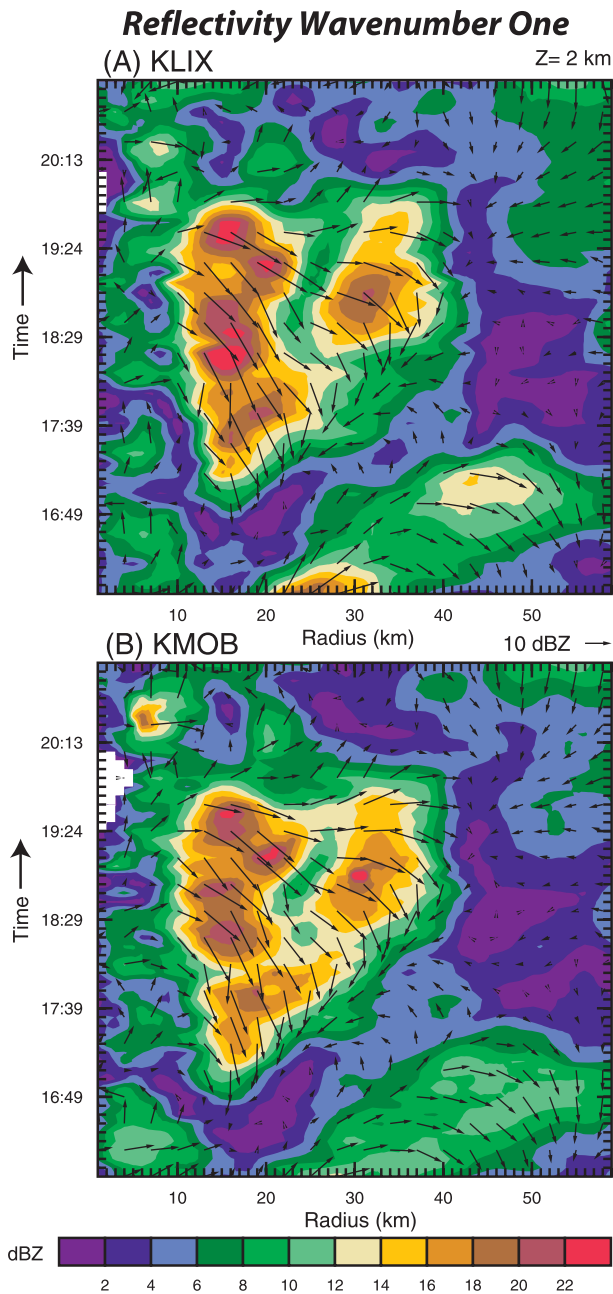## Reflectivity Wavenumber One

(A) KLIX

(B) KMOB

FIG. 9. Time–radius (Hovmöller) plot of Hurricane Danny reflectivity wavenumber 1 for (a) KLIX and (b) KMOB at 2 km. The vectors represent the phase of wavenumber 1 of each radius and time where the vector length (direction) represents the wavenumber-1 amplitude (location relative to the center). The vectors point in the direction of the asymmetry, and the magnitude is in dBZ. KMOB depicts weaker reflectivity dBZ values than KLIX.

Tangential Wind Wavenumber Zero

(A) KLIX

(B) KMOB

FIG. 10. Time–radius (Hovmöller) plot of GBVTD-derived mean tangential wind (m s^{-1}) wavenumber 0 for (a) KLIX and (b) KMOB.

uncertainty in the GBVTD-derived axisymmetric V_T is ~7% in Danny. Several possibilities that may contribute to these differences are examined later.

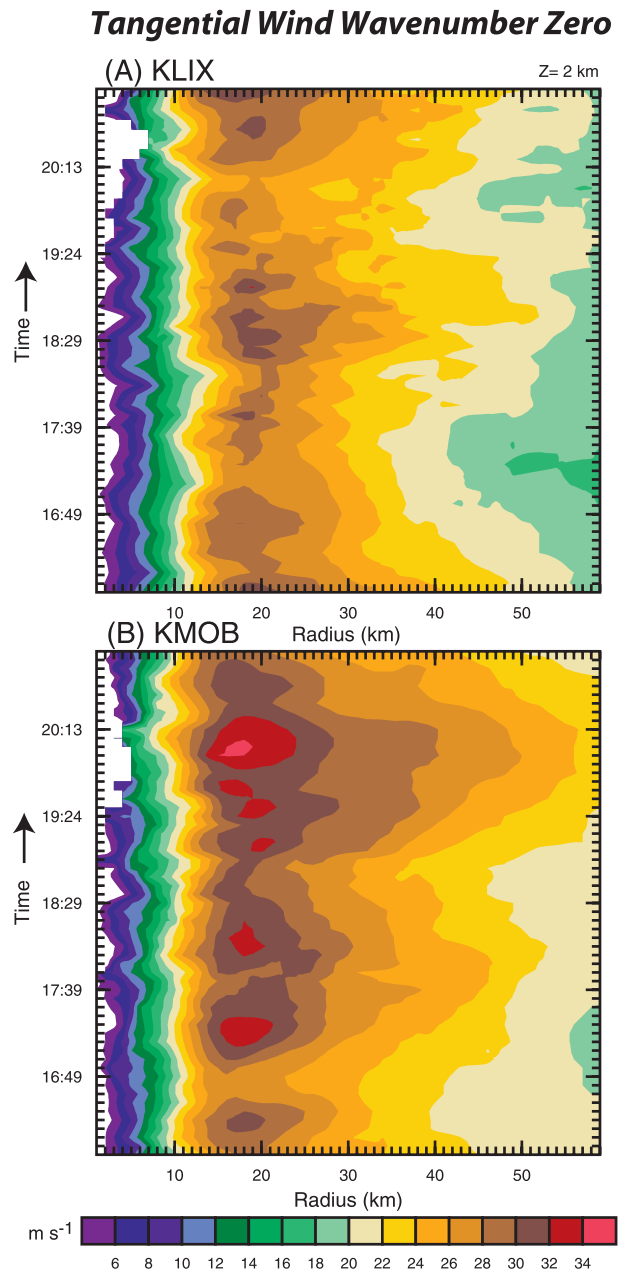Figure 10 shows Danny's wavenumber-1 V_T, whose amplitude and phase are represented by the length and direction of each vector as shown in Fig. 9. The consistency between the KLIX and KMOB derived wavenumber-1 V_T is not as good as anticipated, indicating the challenge to deduce reliable small-amplitude asymmetric components in Danny. The KLIX analysis (Fig. 11a), in general, shows a slightly stronger wavenumber-1 asymmetry in V_T than the KMOB analysis (Fig. 11b). In both analyses, several episodes of enhanced wavenumber-1 V_T near the RMW are apparent. The enhancement between
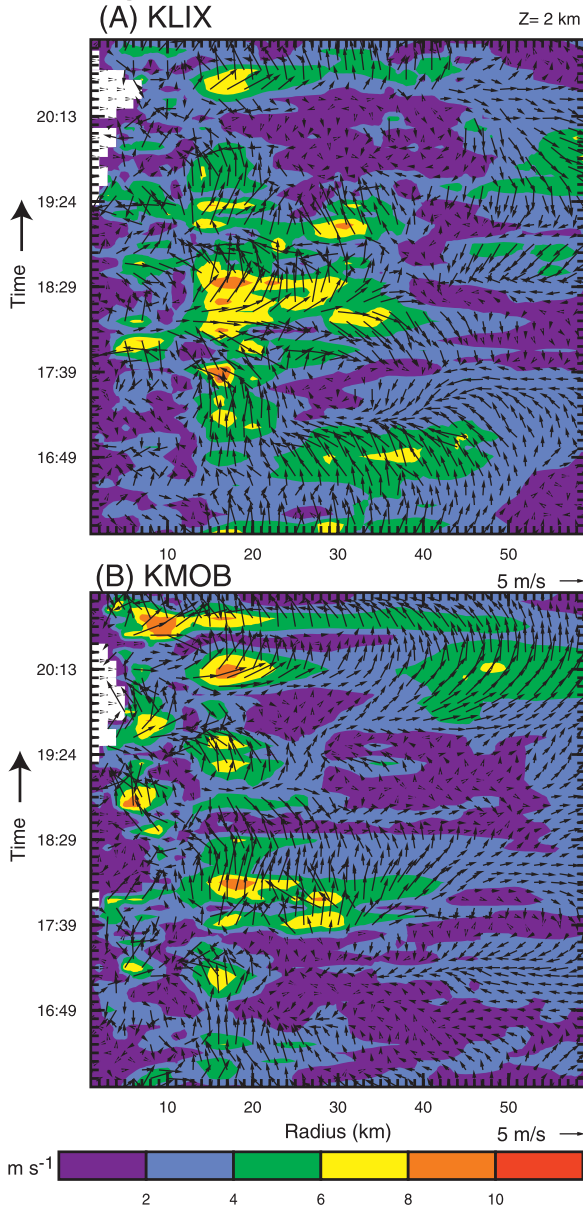
Tangential Wind Wavenumber One

FIG. 11. As in Fig. 10, but for wavenumber 1.

corresponding wavenumber-1 reflectivity (cf. Figs. 9a and 11a). The anticorrelation between the wavenumber-0 and wavenumber-1 V_T in the KMOB and KLIX analyses may be related to how the total winds are decomposed into different wavenumbers. The phase and amplitude of the wavenumber-1 V_T possess a much wider area of small-scale variations than those of the corresponding reflectivity and wavenumber 0, confirming that asymmetric winds are more sensitive to the center location and the uncertainties in the data and aliasing in the GBVTD formulation than their axisymmetric counterparts.

c. Structural comparison and discussion

Throughout the 5-h analysis period, KLIX and KMOB sampled Danny nearly from perpendicular vantage points. Since radial velocity can only be measured along the radar beam, these two radars therefore sampled nearly orthogonal components of Danny's circulation. Because reflectivity is a scalar, it is not a surprise that the KLIX and KMOB reflectivity patterns agree much better than the GBVTD-derived velocity vectors that involve several assumptions and is sensitive to both viewing angle and TC centers. These two datasets and analyses provide a unique opportunity to evaluate the uncertainties embedded in the GBVTD analyses. Two times are chosen to closely examine the characteristics of the GBVTD-derived circulation of Danny. The first time is 1832 UTC, when the values of the axisymmetric V_T for both radars are nearly identical at all radii. The second time is 1954 UTC, when the axisymmetric V_T differs by ~4 m s^{-1} (Fig. 3d).

Both radars show a similar reflectivity pattern at 1832 UTC (in contours) in the 2-km CAPPI (Figs. 12a,b). The TC center is about ~90 km from each radar. A small area exceeding 50 dBZ is seen in the southern half of the storm. This feature is part of the primary eyewall. A secondary reflectivity maximum (>35 dBZ) is seen in the northern quadrant. The velocity pattern at 2-km altitude as seen by both radars indicates that the most intense winds (~33 m s^{-1}) are located in the south to the southeast of the center, consistent with the reflectivity maxima.

The wavenumber-1 asymmetric structure in Danny is depicted in the GBVTD analysis (Figs. 12c,d). The reflectivity (shown in 10-dBZ contours) for both radars has a similar pattern showing positive (negative) anomalies in the southeast (northwest) quadrant. Although the patterns of the azimuthal wavenumber-1 V_T (in color) are consistent with each other, the magnitude is different, with KLIX possessing larger amplitude than the KMOB. Beyond $R = 30$ km, the peak of the wavenumber-1 V_T has shifted to the northwest side of storm. Nevertheless, the KMOB wavenumber-1 amplitude is generally weak (<4 m s^{-1}). There is a concentrated area of V_T (8 m s^{-1})

approximately 1700 and 2000 UTC coincides with the enhancement in the wavenumber-1 reflectivity (Fig. 9) and a general trend of weaker wavenumber-0 amplitude in reflectivity (Fig. 8), further suggesting that Danny evolved from an axisymmetric storm into asymmetric storm during this period. A maximum wavenumber-1 $V_T > 8$ m s^{-1} is seen around the RMW from both radars. The KLIX analysis depicts a more widespread maximum (V_T values >6 m s^{-1}), extending beyond $R = 30$ km, than the KMOB analysis. However, the KLIX wavenumber-1 V_T shows a better correlation with its
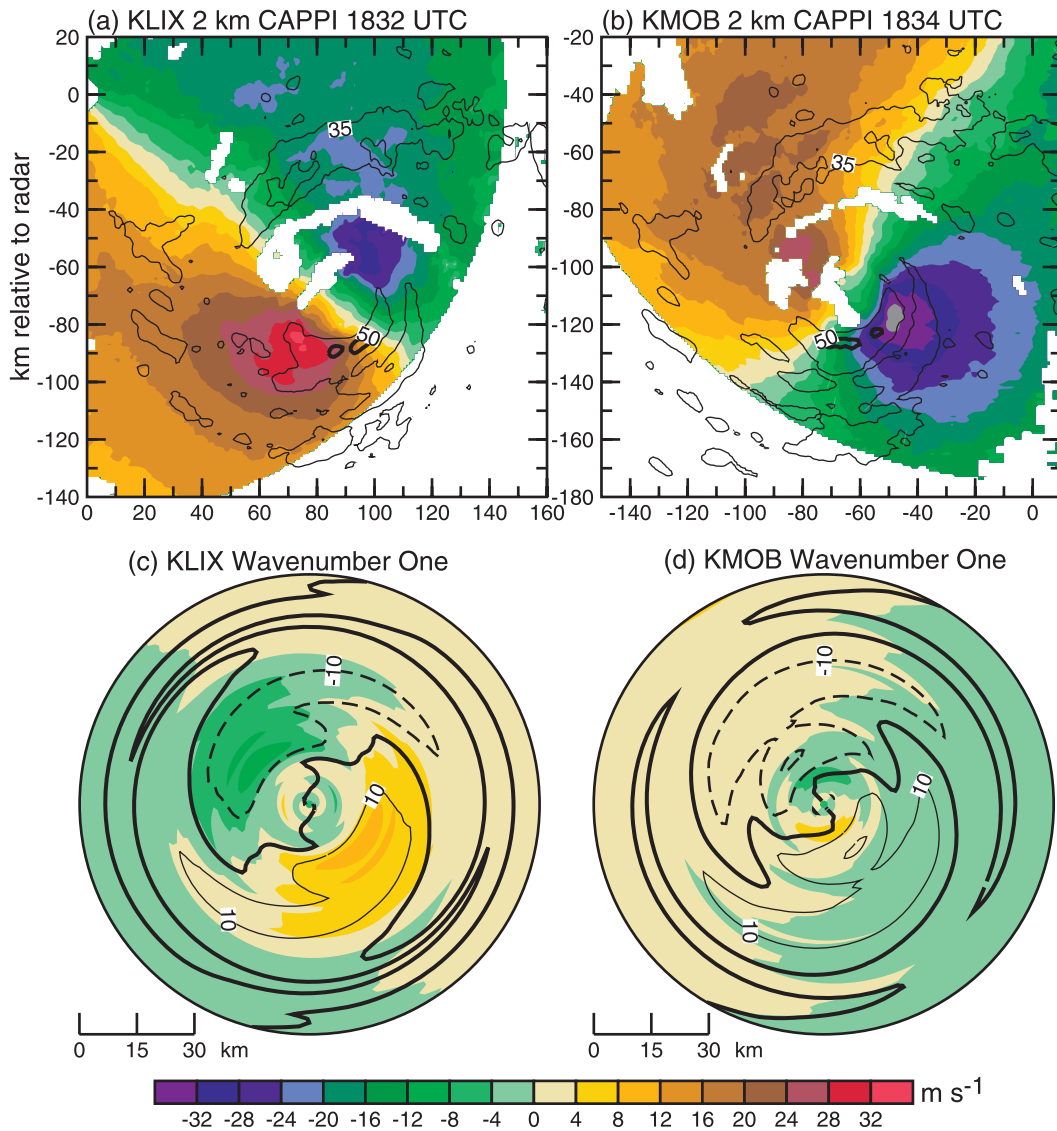
FIG. 12. Comparison of GBVTD results from (left) KLIX radar at 1832 UTC and (right) KMOB at 1834 UTC at 2-km height. (a),(b) The CAPPI radial velocity in color (m s^{-1}) and the 35-dBZ (thin solid line) and 50-dBZ (thick solid line) reflectivity contours. (c),(d) The azimuthal wavenumber-1 tangential velocity in color, and reflectivity with 10-dBZ contours. The bold contour is 0 dBZ.

that coincides with the reflectivity maxima as seen by KLIX, while KMOB barely detects it.

The wavenumber-0 V_T from both radars are in good agreement (Fig. 13a). Both KLIX and KMOB GBVTD analyses (Fig. 13) demonstrate a maximum axisymmetric V_T of 33 m s^{-1} at 20 and 15 km from the center, respectively. The difference in the RMW can also be seen in the axisymmetric reflectivity (Fig. 13b). The reflectivity and V_T values decreased quicker past the RMW in the KLIX analysis compared to the KMOB analysis. In the KMOB analysis, the range of reflectivity and V_T between $R = 15$ and 20 km is ~1 dBZ and 1 m s^{-1}. Hence, the

KMOB center was chosen with an RMW of 18 km, rather than the peak wavenumber-0 V_T at 15 km, based on the criterion of the storm structure continuity. Other than this, the reflectivity wavenumber-0 fields vary, but have a similar overall pattern. Two distinct peaks are seen by KMOB (Fig. 13b). The secondary peak at around 45 km appeared in the KMOB analysis but is much broader in the KLIX analysis.

Figure 14 compares the derived total wind speed at 2 km from a dual-Doppler analysis with GBVTD-derived total winds from KLIX and KMOB. The dual-Doppler analysis is considered the ground truth (Fig. 14a). The
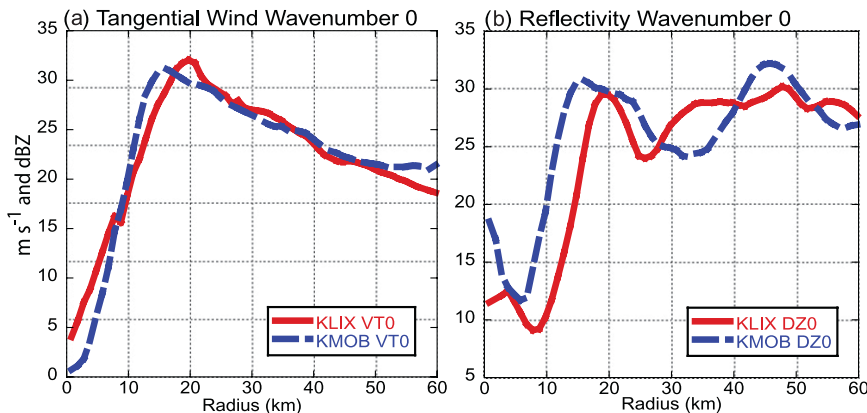
FIG. 13. Comparison of GBVTD results for KLIX and KMOB at 1834 UTC. The azimuthal wavenumber-0 tangential (a) velocity and (b) reflectivity.

dual-Doppler analysis is deduced from a fully three-dimensional variational technique, which solves the dual-Doppler equations (two dual-Doppler projection equations for zonal and meridional velocity using an estimate for the total vertical velocity) and the anelastic continuity equation simultaneously (Gamache 1997; Reasor et al. 2009). Both GBVTD analyses (Figs. 14b,c) resemble the dual-Doppler analysis (Fig. 14a). All three analyses show the maximum wind speed located in the southeast quadrant, consistent with the reflectivity maximum (black contours in Fig. 14a). The GBVTD-derived centers (shown in Fig. 14a) used for each GBVTD analyses are close to the circulation center used for the dual-Doppler analysis. The RMW remains consistent for all three analyses. The magnitude of the wind speed is larger in KLIX (Fig. 14b) than in the KMOB or dual-Doppler analyses. The KLIX CAPPI (Fig. 12a) reveals a stronger outbound radial velocity max than KMOB. This result is also consistent with the azimuthal wavenumber-1 V_T plot shown in Fig. 12c for KLIX. Danny was closer to the KLIX radar at this time and may have detected features in the storm not seen by the KMOB. In addition, the much smaller analysis domain in the dual-Doppler analysis (Fig. 14a) is an apparent limitation compared with both of the GBVTD analyses (Figs. 14b,c).

An hour and 20 min later (at 1954 UTC), Hurricane Danny's structure changed significantly. The eyewall reflectivity weakened at the end of the period of enhanced wavenumber-1 component (Fig. 9) and the intensification of the wavenumber-0 component (Fig. 8). The maximum reflectivity appeared in the north-to-northeast quadrant and a rainband spiraled clockwise outward and formed a broad arc of >35 dBZ in the southwest quadrant (Figs. 15a,b). The KLIX CAPPI reveals two areas of outbound (relative to radar location) velocities of 24 m s^{-1} associated with the eyewall and the outer rainband. The

typical hurricane inbound radial velocity pattern is seen from KMOB (Fig. 15b), while a weaker radial flow is shown from KLIX (Fig. 15a). This multiple maxima Doppler velocity pattern, especially only existing on the inbound or outbound side, can confuse the GBVTD-simplex algorithm because the maximum outbound Doppler velocity can be paired with either inbound Doppler velocity maximum from different centers in the original GBVTD-simplex algorithm. Applying the time continuity constraints alleviated this problem.

The reflectivity wavenumber-1 (in contours) pattern is also similar for both (Figs. 15c,d) but the magnitude is weaker than that shown in the previous example. The wavenumber-1 V_T for both radars have similar features near the storm center with two areas ±8 m s^{-1} directly north and south of the center (Fig. 15d). There are two other areas of ±8 m s^{-1} at 60 and 45 km from the center for KLIX and KLOB, respectively. The azimuthal wavenumber-0 V_T for KLIX and KMOB have a similar pattern with a slight offset of the peak wind (Fig. 16a). This time KMOB shows a maximum of 33 m s^{-1} at 18 km from the center while KLIX peaks at 28 m s^{-1} at 18 km. There is also a nearly constant offset of ~6 m s^{-1} beyond the RMW. The reflectivity wavenumber-0 patterns are nearly identical with the peak reflectivity located at $R = 17$ km (Fig. 16b).

Comparisons of the GBVTD analyses from both radars to the dual-Doppler for 1954 UTC are demonstrated in Fig. 15. Although there are broad similarities such as the RMW and the wind speed maximum on the northeast or east side of the storm, there are some notable differences in the other quadrants. These differences are not too distressing given that the V_{T0} from both radars shown in Fig. 16a are off. Several possible reasons that may cause the inconsistency between two GBVTD analyses are discussed in the next section.
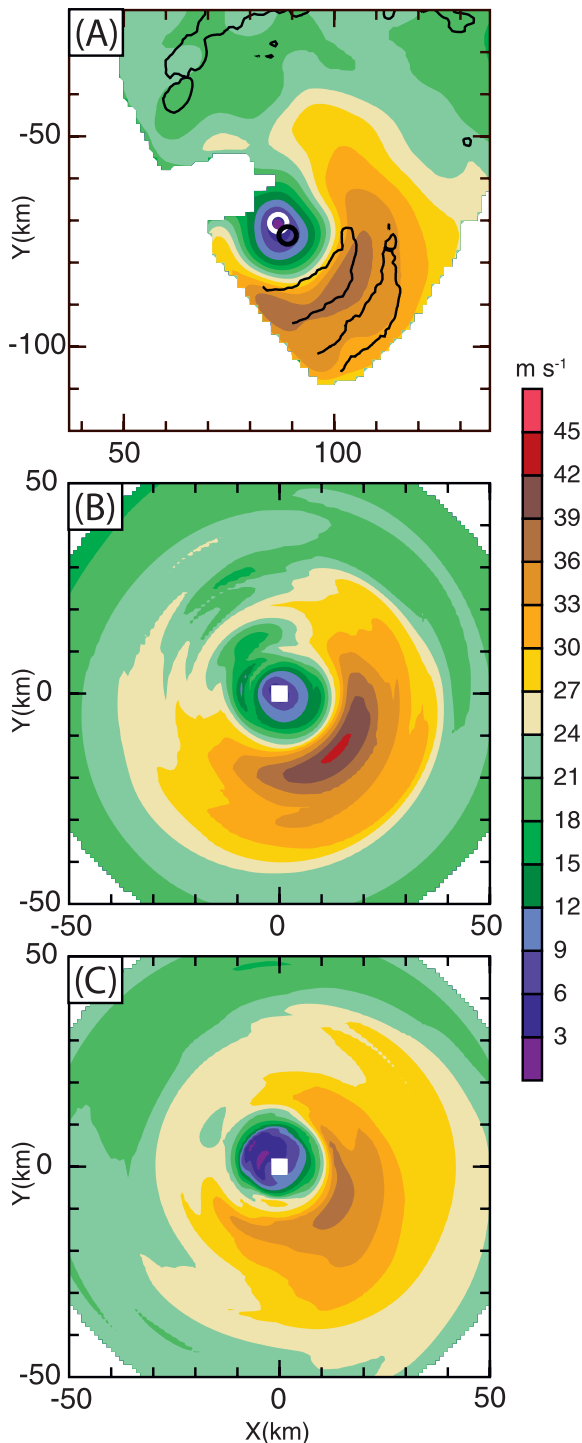
FIG. 14. Derived total wind speed (color, m s^{-1}) from (a) dual-Doppler analysis and GBVTD analysis of (b) KLIX and (c) KMOB radar data from Hurricane Danny at 1832 UTC at 2 km. The solid black lines in (a) denote the 40-dBZ reflectivity contours, with white circle indicating position of the center used in (b), and black circle indicating center used in (c). Cartesian distances are from KLIX radar in (a), and from GBVTD-derived centers in (b) and (c). The dual-Doppler analysis is considered the "ground truth."

5. Value of high-frequency analyses for monitoring storm evolution

Estimates of the circulation center location and kinematic structure of the eyewall are available every 6 min for 5 h. Such a high temporal frequency enables a detailed evaluation of the evolution of the storm center, wind, and reflectivity fields that has been impossible in past studies. A future paper will examine this evolution is detail, but we shall make a few preliminary comments on the GBVTD-derived analyses here.

The circulation center is well approximated by a linear regression (Fig. 3b, with R2 ≥ 0.9). Deviations from a linear fit are short lived, 6–12 min, and are of small spatial extent, about 2 km or about one-tenth the horizontal scale of the RMW. Trochoidal motion or wobbles of the circulation center, detected for several other TCs (e.g., Jordan and Stowell 1955; Jordan 1966; Willoughby and Chelmow 1982; Muramatsu 1986b; Roux and Viltard 1995; Marks et al. 2008) can have periods ranging from 20 min to more than 12 h. Nolan et al. (2001) argue that the cause of such wobbles, which can be observed in their three-dimensional dry hurricane-like vortex model on time scales as short as 20 min, is possibly due to mixing of low vorticity air into the high vorticity annulus of the eyewall. In Danny, trochoidal motions are either not present or so small as to be inconsequential, at least for the 5 h of sampling (Fig. 3b, KMOB centers). The lack of trochoidal motion may be caused by inherent uncertainties associated with the GBVTD-simplex technique resulting from the intrinsic assumptions in GBVTD (Lee et al. 1999). As seen in Fig. 9, Danny's reflectivity became dominated by a wavenumber-1 asymmetry during the middle part of the study period (1700–2000 UTC), with the vectors pointing toward the southeast. Despite the presence of this pronounced asymmetry, there is not a distinct signature of trochoidal motion. The V_T (Fig. 11) also does not show any hint of such motions. This suggests that the presence (or absence) of trochoidal motions is not directly related to convective asymmetries, during this time. Hence and Houze (2008), suggested that the presence of a wavenumber-1 low-level wind maximum is related to the processes of convective mass transport. Based on what is demonstrated in Figs. 9 and 11, there is not a clear relationship between the asymmetric wind maximum and convective mass transport. If we use the reflectivity as a proxy for convective mass transport, it can be seen that there is not a direct relationship between the timing of the wavenumber-1 asymmetry in reflectivity with the asymmetry in V_T (i.e., when the reflectivity is dominated by wavenumber 1, the V_T does not show the same signature). Furthermore, the phase of the reflectivity asymmetry (Fig. 9) remains fixed toward the southeast
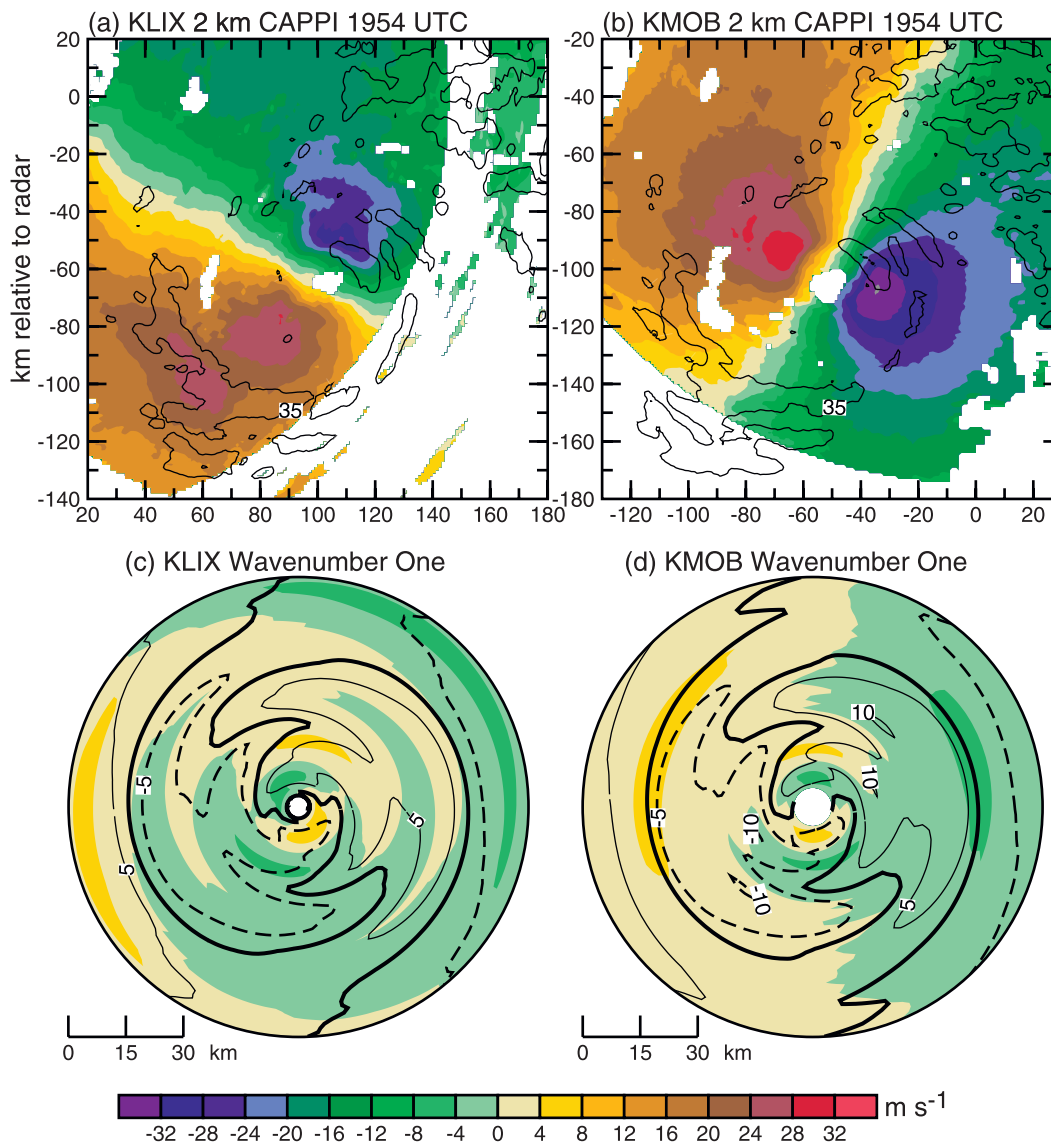
FIG. 15. As in Fig. 12, but at 1954 UTC. (c),(d) Reflectivity contours are 5 dBZ because of the weaker wavenumber-1 magnitude at this time.

side of the storm, whereas the phase in the V_T asymmetry varies over multiple directions, suggesting that these asymmetries are not phase locked. An examination of the GBVTD-derived centers for KLIX and KMOB for the entire time that Danny is within 150 km range of either radar, a little over 5 days, may reveal if trochoidal motions are present for longer temporal scales.

The GBVTD analysis reveals a wavenumber-1 reflectivity pattern in the eyewall from about 1715 to 1945 UTC (Fig. 9). The magnitude exceeds 20 dBZ for both radars from about 1815 to 1940 UTC. This maximum in reflectivity moves slowly ($\sim$3 m s^{-1}) from the south-southeast to the east portion of the eyewall over 2.5 h

(Fig. 9, vectors). There is also a wavenumber-1 wind maximum (6–8 m s^{-1}) that is generally collocated with the maximum in reflectivity during the early stage of the asymmetry (Figs. 12 and 14). Later, the wavenumber-1 asymmetry tends to be downstream of the weakened reflectivity maximum (Figs. 15 and 17). The increase of the tangential winds is initially correlated with increased convection in the southeast quadrant. The wind then becomes relatively smooth in the eyewall as the convection dissipates. Higher tangential winds in the lower troposphere have been correlated with reflectivity features, presumed to be convective cells, in rainbands (Barnes et al. 1991) and in the eyewall (Marks et al. 1992).
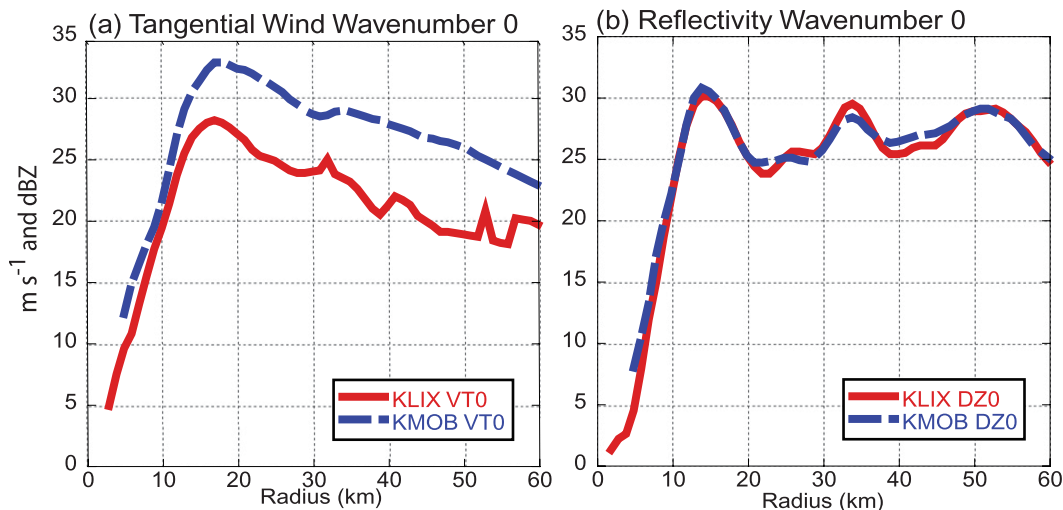
FIG. 16. As in Fig. 13, but at 1954 UTC.

Despite the appearance of the aforementioned wavenumber-1 pattern the RMW and the mean tangential winds are remarkably steady (Fig. 3d). The RMW decreases slightly from 18 to 17 km and the mean tangential winds decrease from 33 to 31 m s^{-1} at 2-km altitude over 5 h. During this period the best-track record reveals that MSLP deepens ~3 hPa. There is no hint of development of concentric eyewalls in Danny that are believed to exist later when the TC is over Mobile Bay (Blackwell 2000). The GBVTD-derived mean fields, obtained with such high temporal resolution, provide a superior method of monitoring the evolution of the eyewall. Application of the technique will provide the details of TCs as they make landfall, a time when aircraft reconnaissance may be limited.

6. Error sources in estimating mean tangential wind

The additional constraints (described in section 4) applied in this study have significantly reduced the uncertainty of the original GBVTD-simplex-derived TC centers from ~2 to ~1.5 km, consistent with the requirement proposed and the estimated uncertainty in Typhoon Alex (1987) in LM00. It is apparent that the GBVTD-derived structures of Danny using the improved center estimates are quite plausible and generally in agreement with the dual-Doppler synthesis. However, the reduced center uncertainty is unable to decrease the systematic differences of the V_T between the KLIX and KMOB analyses (cf. Fig. 10). This merits further discussion. In addition to the remaining uncertainties in center location, the disagreement between V_T in these two GBVTD analyses may be attributed to the following reasons: 1) sampling differences from the

individual radars including differences in horizontal and vertical data coverage and 2) unresolved asymmetric radial winds and cross-beam mean wind.

As Danny moved eastward across the radar sampling domain, different parts of the storm were sampled due to the limited Doppler range, discrete sampling in the vertical, and sampling from different vantage point (e.g., Figs. 12a,b and 15a,b). In addition, the resolution and altitude of the radar beam is a function of distance and is affected by the earth's curvature. These aforementioned factors can contribute to the differences in GBVTD-retrieved storm structures. Unfortunately, it is very difficult to quantify the impact from these factors in this dataset and ''reduce'' the uncertainty in this respect.

Next, the impacts of the unresolved cross-beam mean wind and the sine component of the wavenumber-2 radial wind on the mean tangential winds are discussed. The GBVTD-derived wavenumber-0 tangential wind (V_{T0}) has the following form [Eq. (20) in Lee et al. (1999)]:

$$V_{T0} = -B_1 - B_3 - V_M \sin(\theta_T - \theta_M)\sin\alpha_{max} + V_R S_2.$$
(1)

The third and fourth terms on the right-hand side (rhs) of (1) represent the unresolved cross-beam mean wind and the unknown wavenumber-2 radial wind. These two terms have been set to zero as the closure assumptions in previous GBVTD studies because they cannot be estimated from single-Doppler observations. With simultaneous observations from KLIX and KMOB, the cross-beam mean wind and the wavenumber-2 component can be estimated.

The cross-beam mean wind can be resolved by radar observations from two different vantage points from the along beam mean flow:

$$V_M \cos(\theta_{T_{\text{MOB}}} - \theta_M)$$
$$= (A_0 + A_2 + A_4 - V_R C_1 - V_R C_3)_{\text{MOB}} = A \qquad (2)$$

$$V_M \cos(\theta_{T_{\text{LIX}}} - \theta_M)$$
$$= (A_0 + A_2 + A_4 - V_R C_1 - V_R C_3)_{\text{LIX}} = B. \qquad (3)$$

The direction of the mean wind flow, θ_M, and the magnitude of the mean flow V_M can be solved as follows (interested reader can find the full derivation in the appendix):

$$\theta_M = \tan^{-1}\left(\frac{B\cos\theta_{T_{\text{LIX}}} - A\cos\theta_{T_{\text{LIX}}}}{A\sin\theta_{T_{\text{LIX}}} - B\sin\theta_{T_{\text{LIX}}}}\right), \qquad (4)$$

$$V_M = \sqrt{\left(\frac{A\cos\theta_{T_{\text{LIX}}} - B\cos\theta_{T_{\text{MOB}}}}{\sin\theta_{T_{\text{MOB}}}\cos\theta_{T_{\text{LIX}}} - \cos\theta_{T_{\text{LIX}}}\sin_{T_{\text{LIX}}}}\right)^2 + \left(\frac{A\sin\theta_{T_{\text{LIX}}} - B\sin\theta_{T_{\text{MOB}}}}{-\sin\theta_{T_{\text{MOB}}}\cos\theta_{T_{\text{LIX}}} + \cos\theta_{T_{\text{MOB}}}\sin\theta_{T_{\text{LIX}}}}\right)^2}. \qquad (5)$$

It can be seen that the unknown $V_R C_1$ and $V_R C_3$ will bias the resulting θ_M and V_M. Figure 18 demonstrates θ_M at 2-km altitude. The angles 45°, 0°, and −45° are northeast, east, and southeast, respectively. The direction of the mean wind flow in Danny possesses an easterly component except around 1923 UTC, where θ_M changes sharply, and then returns to the similar pattern as seen in early periods. Figure 19 illustrates the magnitude of the along beam V_M from KLIX and KMOB at 2-km altitude. KLIX (KMOB) sensed a positive (negative) along beam V_M, consistent with the general eastward movement of Danny. The mean wind magnitude fluctuated between 1 and 5 m s^{-1} (not shown), which is relatively weak and consistent with the slow motion of Danny. Figure 20 displays the derived cross-beam mean wind V_X for both radars. Throughout the period, V_X fluctuates but the magnitude is in general less than 1 m s^{-1}, hence, the V_X component projected onto each radial has minimal impact on V_T and cannot explain the 5 m s^{-1} difference between 1900 and 2030 UTC in Fig. 3c.

Though Danny is dominated by wavenumber 1 between 1700–1930 UTC, the wavenumber-2 component is nonnegligible as shown in Fig. 21. Since the viewing angles from KMOB and KLIX are nearly 90° apart, the aliasing effect from the wavenumber-2 radial winds to the V_T deduced from these two radars would be out of phase. While there is ongoing research attempting to improve the closure assumption on the asymmetric structures (e.g., Lee et al. 2006), an accurate partition of the total wavenumber-2 amplitude into its tangential and radial components is still not satisfactory. The peak total wavenumber-2 amplitude between 4 and 6 m s^{-1} suggest that a radial wind asymmetry may have sufficient amplitude to account for most of the 5 m s^{-1} bias in Danny.

7. Summary and future work

Previous ground-based velocity track display (GBVTD) studies (Lee et al. 2000; Harasti et al. 2004) highlighted

the significance of obtaining an accurate circulation center in order to derive a realistic asymmetric circulation from the technique. LM00 stressed that the circulation center of a TC needs to be accurately determined within 5% of its radius of RMW in order to retrieve acceptable asymmetric structures. However, previous studies could not quantitatively evaluate the accuracy of either the GBVTD-simplex-derived circulation centers or the GBVTD-derived wind fields. In the Hurricane Danny (1997) case the sensitivity of the GBVTD solutions were evaluated using simultaneous observations by two coastal WSR-88D radars (KMOB and KLIX) every 6 min for 5 h. The two radars sampled the circulation center from nearly perpendicular vantage points providing essentially two independent looks of Danny. This dataset provided a unique opportunity to quantitatively evaluate the GBVTD center-finding technique and the GBVTD-retrieved TC structures. With two Doppler radars observing the same storm, the mean wind magnitude V_M, the direction of the mean wind θ_M, and the cross-beam component V_X were derived to evaluate the effects of the unknown cross-beam mean wind in determining the storm structures.

These two sets of Danny's centers, computed from the KLIX and KMOB data using the original GBVTD-simplex method, were generally consistent with each other with a mean difference of 2.1 km and a standard deviation of 1.2 km. Although these uncertainties were in line with estimates cited in previous studies, examining the retrieved TC characteristics (e.g., RMW, mean tangential winds, and center locations) revealed that unreasonably large fluctuations existed for successive periods. It is shown that the mean difference (standard deviation) between these two sets of centers was reduced to 1.6 (1.0) km by 1) including asymmetric components (wavenumber 1 in Danny) in the GBVTD-simplex curve fit and 2) implementing physical constraints so the key TC characteristics are consistent in both space and time. Implementing these two additional constraints in the GBVTD-simplex algorithm drastically improved the
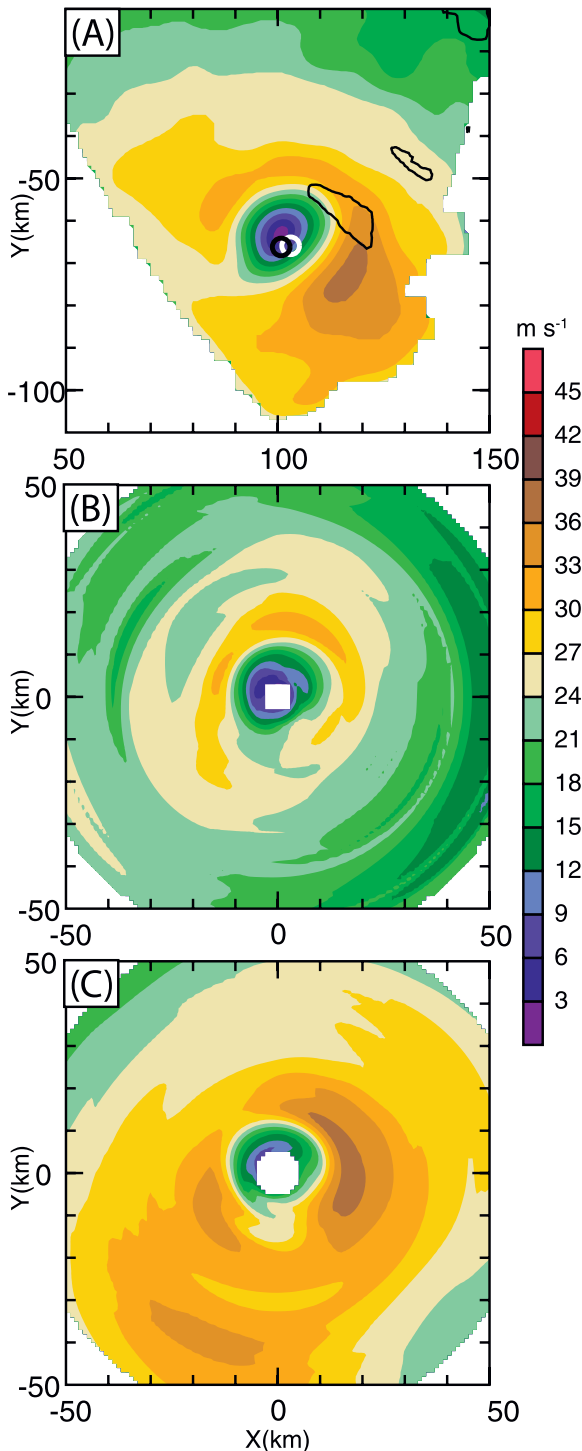
FIG. 17. As in Fig. 14, but for 1954 UTC.

FIG. 18. The direction of the mean wind flow θ_M derived from (4). The angles 45°, 0°, and −45° are pointing toward the northeast, east, and southeast, respectively, as in Lee et al. (1999).

stability and consistency of the retrieved TC center and subsequently retrieved more physically plausible kinematic structures in Hurricane Danny.

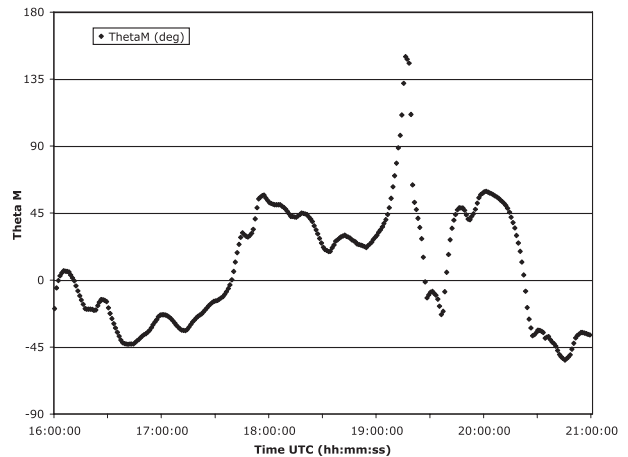Danny's kinematic structures were retrieved from KLIX and KMOB data using the improved sets of centers and compared with each other in the wavenumber domain in the TC-centered cylindrical coordinates. The reflectivity (a scalar) showed the best agreement. Danny evolved from a mostly axisymmetric TC into a wavenumber-1 asymmetric TC then returned to an axisymmetric TC during this period. The mean tangential winds between these two analyses show general agreement in magnitude and the RMW. Noticeable differences appeared as an out of sinusoidal variation in magnitude ($\sim$3 m s^{-1}) around a mean value of $\sim$31 m s^{-1} between 1900 and 2030 UTC. This variation is $\sim$10% of the axisymmetric circulation. This feature may be a result of the aliasing from the unresolved cross-beam mean wind and/or the sine component of the wavenumber-2 radial wind. In Danny, the retrieved cross-beam mean wind is small and is not able to account for the differences in the derived mean tangential winds while the surges of wavenumber 2 with peak amplitude $\sim$(4–6) m s^{-1} are capable of producing these variations in the mean tangential winds. Future studies on GBVTD closure assumptions (i.e., partitioning total asymmetric amplitudes into tangential and radial) are required to fully investigate this possibility.

This study provides a quantitative evaluation of the GBVTD-simplex-derived TC centers, RMWs, and mean tangential winds using two WSR-88D radars from two vantage points. The overall uncertainty of the GBVTD-simplex and the GBVTD algorithms is consistent with the theoretical and practical limits speculated in previous studies. This study also revealed some interesting differences in the GBVTD-retrieved TC structures that cannot be eliminated by implementing additional physical constraints to the algorithms. Hence, the uncertainties illustrated in this study may be the "practical" limits one can
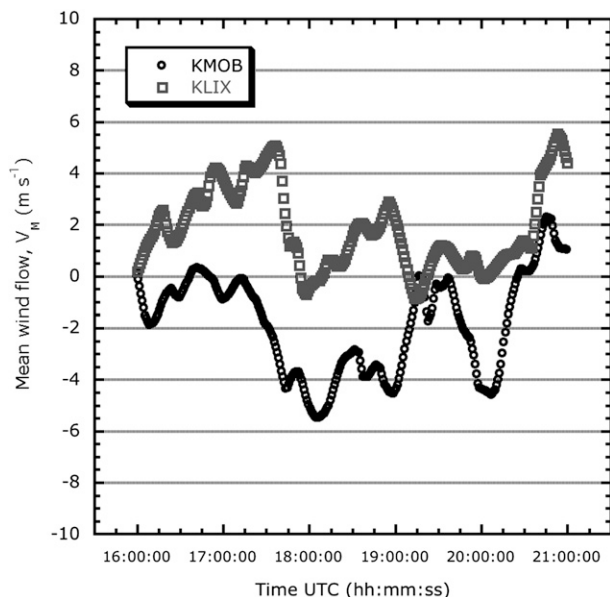
FIG. 19. The mean wind flow V_M for KLIX and KMOB.

FIG. 21. Time series of wavenumber-0 tangential wind (left axis, black and blue curves) and wavenumber-2 amplitude (right axis, red and green curves) from KLIX and KMOB GBVTD retrieval.

expect by using the GBVTD-simplex and the GBVTD algorithms using the current NEXRAD scanning strategy.

Algorithms such as the hurricane volume velocity processing (HVVP; Harasti 2003) and generalized velocity track display GVTD (Jou et al. 2008) have shown encouraging results in estimating the full mean wind from single-Doppler radar data and can be incorporated into the improved GBVTD-simplex and the G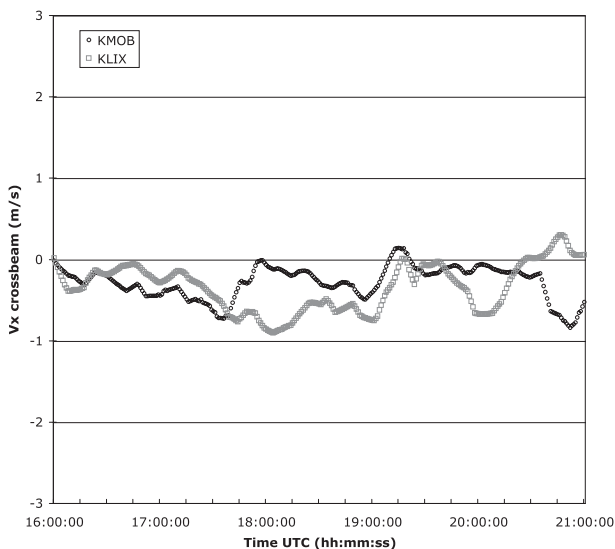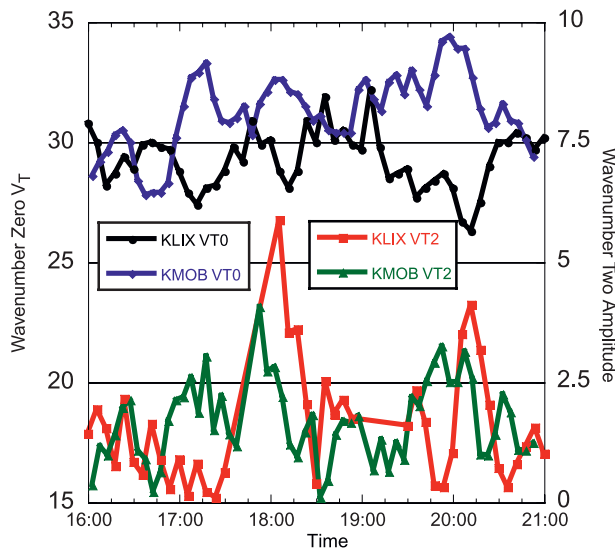BVTD algorithm. Attempts to improve the closure assumptions are ongoing research topics (e.g., Lee et al. 2006). More importantly, the improved GBVTD-simplex algorithm presented in this study requires interactive selection of best centers by examining time continuity of several key TC characteristics and cannot be used in operational environments in its current form. The procedures described in this study have been combined with the HVVP (Harasti 2003) to form the basis of the vortex objective radar tracking and circulation (VORTRAC) software package to deduce circulation center and central pressure of landfall TCs at the National Hurricane Center in real time. A research version of VORTRAC is currently under development that will provide the capability for researchers to efficiently process large quantities of WSR-88D data for landfalling TCs in the future.

FIG. 20. The V_X (cross-beam component) of V_M derived from KLIX and KMOB.

APPENDIX

Derivation of the Mean Wind from Two Radars

By examining the GBVTD equations, the mean tangential wind [Eq. (20) in Lee et al. (1999)] is affected by the unknown cross-beam mean wind and the unknown wavenumber-2 radial wind. Here we examine the effects of the unknown cross-beam mean wind V_X to the mean tangential wind. Since two independent Doppler radars sampled Hurricane Danny, this provides a unique opportunity to solve for the mean wind flow V_M and evaluate the effect of V_X.

Taking Eq. (19) from Lee et al. (1999)

$$V_M \cos(\theta_T - \theta_M) = A_0 + A_2 + A_4 - V_R C_1 - V_R C_3, \quad (A1)$$

where θ_T is the mathematical angle (i.e., 90°N, 0°, etc.) for the tropical cyclone center viewed from the radar; θ_M is the direction of the mean wind flow, which is a function of altitude; A_N and C_N are Fourier coefficients of wavenumber N for the intersections of the radar beam and a ring of radius R; and V_R is the radial velocity of the TC, positive outward from the center. See Fig. 1 and appendix A of Lee et al. (1999) for a complete description of the geometry of the GBVTD technique.

In this formulation, the left-hand side of (A1) is referred to as the along beam V_M and the rhs represents general expressions between the observed Doppler velocities and the tangential and radial winds on a GBVTD ring [see Eqs. (13)–(18) of Lee et al. 1999]. Rewriting it for both radars KMOB (MOB) and KLIX (LIX) yields

$$V_M \cos(\theta_{T_{MOB}} - \theta_M)$$
$$= (A_0 + A_2 + A_4 - V_R C_1 - V_R C_3)_{MOB}, \quad (A2)$$

$$V_M \cos(\theta_{T_{LIX}} - \theta_M)$$
$$= (A_0 + A_2 + A_4 - V_R C_1 - V_R C_3)_{LIX}. \quad (A3)$$

Renaming the rhs in (A2) and (A3), we get

$$V_M \cos(\theta_{T_{MOB}} - \theta_M) = A, \quad (A4)$$

$$V_M \cos(\theta_{T_{LIX}} - \theta_M) = B. \quad (A5)$$

Applying the cosine trig identity: $\cos(x - y) = \cos x \cos y + \sin x \sin y$ for (A4) and (A5), we get

$$V_M(\cos\theta_{T_{MOB}} \cos\theta_M + \sin\theta_{T_{MOB}} \sin\theta_M) = A, \quad (A6)$$

$$V_M(\cos\theta_{T_{LIX}} \cos\theta_M + \sin\theta_{T_{LIX}} \sin\theta_M) = B. \quad (A7)$$

To simplify further, we substitute C, D, E, and F for θ_T terms in (A6) and (A7) and multiply V_M throughout and get

$$V_M C \cos\theta_M + V_M D \sin\theta_M = A, \quad (A8)$$

$$V_M E \cos\theta_M + V_M F \sin\theta_M = B. \quad (A9)$$

Multiply (A8) by E and (A9) by C we get

$$V_M CE \cos\theta_M + V_M DE \sin\theta_M = AE, \quad (A10)$$

$$V_M CE \cos\theta + V_M CF \sin\theta_M = CB. \quad (A11)$$

Multiply (A8) by F and (A9) by D we get

$$V_M CF \cos\theta_M + V_M DF \sin\theta_M = AF, \quad (A12)$$

$$V_M DE \cos\theta_M + V_M DF \sin\theta_M = DB. \quad (A13)$$

Now we have two sets of equations (A10) and (A11) and (A12) and (A13).
Subtracting (A10)–(A11) and (A12)–(A13) to simplify and we get

$$V_M(DE - CF)\sin\theta_M = AE - BC, \quad (A14)$$

$$V_M(CF - DE)\cos\theta_M - AF - DB. \quad (A15)$$

Rearranging (A14) and (A15), we get

$$V_M \sin\theta_M = \frac{AE - BC}{DE - CF}, \quad (A16)$$

$$V_M \cos\theta_M = \frac{AF - DB}{CF - DE}. \quad (A17)$$

Dividing (A16) by (A17) we get

$$\tan\theta_M = \frac{\left(\dfrac{AE - BC}{DE - CF}\right)}{\left(\dfrac{AF - DB}{CF - DE}\right)}. \quad (A18)$$

Simplifying (A18) we get

$$\tan\theta_M = \frac{BC - AE}{AF - DB}. \quad (A19)$$

Solving for θ_M by taking the inverse tangent we get

$$\theta_M = \tan^{-1}\left(\frac{BC - AE}{AF - DB}\right). \quad (A20)$$

Now expand terms C, D, E, and F we get

$$\theta_M = \tan^{-1}\left(\frac{B\cos\theta_{T_{\mathrm{MOB}}} - A\cos\theta_{T_{\mathrm{LIX}}}}{A\sin\theta_{T_{\mathrm{LIX}}} - B\sin\theta_{T_{\mathrm{MOB}}}}\right), \quad (A21)$$

where A and B are the rhs terms from (A4) and (A5).

The magnitude of the mean flow V_M has the following form from (A16) and (A17):

$$V_M = \sqrt{\left(\frac{AE - BC}{DE - CF}\right)^2 + \left(\frac{AF - DB}{CF - DE}\right)^2}$$

$$= \sqrt{\left(\frac{A\cos\theta_{T_{\mathrm{LIX}}} - B\cos\theta_{T_{\mathrm{MOB}}}}{\sin\theta_{T_{\mathrm{MOB}}}\cos\theta_{T_{\mathrm{LIX}}} - \cos\theta_{T_{\mathrm{LIX}}}\sin\theta_{T_{\mathrm{LIX}}}}\right)^2 + \left(\frac{A\sin\theta_{T_{\mathrm{LIX}}} - B\sin\theta_{T_{\mathrm{MOB}}}}{-\sin\theta_{T_{\mathrm{MOB}}}\cos\theta_{T_{\mathrm{LIX}}} + \cos\theta_{T_{\mathrm{MOB}}}\sin\theta_{T_{\mathrm{LIX}}}}\right)^2}.$$

REFERENCES

Bargen, D. W., and R. C. Brown, 1980: Interactive radar velocity unfolding. Preprints, *19th Conf. on Radar Meteorology,* Miami Beach, FL, Amer. Meteor. Soc., 278–285.

Barnes, G. M., J. F. Gamache, M. A. LeMone, and G. J. Stossmeister, 1991: A convective cell in a hurricane rainband. *Mon. Wea. Rev.,* **119,** 776–794.

Blackwell, K. G., 2000: The evolution of Hurricane Danny (1997) at landfall: Doppler-observed eyewall replacement, vortex contraction/intensification, and low-level wind maxima. *Mon. Wea. Rev.,* **128,** 4002–4016.

Crum, T. D., R. L. Alberty, and D. W. Burgess, 1993: Recording, archiving, and using WSR-88D Operational Support Facility. *Bull. Amer. Meteor. Soc.,* **74,** 645–653.

Dodge, P., R. W. Burpee, and F. D. Marks Jr., 1999: The kinematic structure of a hurricane with sea level pressure less than 900 mb. *Mon. Wea. Rev.,* **127,** 987–1004.

Gamache, J. F., 1997: Evaluation of a fully three-dimensional variational Doppler analysis technique. Preprints, *28th Conf. on Radar Meteorology,* Austin, TX, Amer. Meteor. Soc., 422–423.

——, F. D. Marks, and F. Roux, 1995: Comparison of three airborne Doppler sampling technique with airborne in-situ wind observations in Hurricane Gustav (1990). *J. Atmos. Oceanic Technol.,* **12,** 171–181.

Harasti, P. R., 2003: The hurricane volume velocity processing method. Preprints, *31st Conf. on Radar Meteorology,* Seattle, WA, Amer. Meteor. Soc., 1008–1011.

——, C. J. McAdie, P. P. Dodge, W.-C. Lee, J. Tuttle, S. T. Murillo, and F. D. Marks, 2004: Real-time implementation of single-Doppler radar analysis methods for tropical cyclones: Algorithm improvements and use with WSR-88D display data. *Wea. Forecasting,* **19,** 219–239.

Hence, D. A., and R. A. Houze Jr., 2008: Kinematic structure of convective-scale elements in the rainbands of Hurricanes Katrina and Rita (2005). *J. Geophys. Res.,* **113,** D15108, doi:10.1029/2007JD009429.

Jordan, C. L., 1966: Surface pressure variations at coastal stations during the period of irregular motion of Hurricane Carla of 1961. *Mon. Wea. Rev.,* **94,** 454–458.

Jordan, H. M., and D. J. Stowell, 1955: Some small scale features of the track of Hurricane Ione. *Mon. Wea. Rev.,* **83,** 210–215.

Jou, B. J.-D., W.-C. Lee, S.-P. Liu, and Y.-C. Kao, 2008: Generalized VTD (GVTD) retrieval of atmospheric vortex kinematic structure. Part I: Formulation and error analysis. *Mon. Wea. Rev.,* **136,** 995–1012.

Lee, W.-C., and F. D. Marks, 2000: Tropical cyclone kinematic structure retrieved from single Doppler radar observations.

Part II: The GBVTD-simplex center finding algorithm. *Mon. Wea. Rev.,* **128,** 1925–1936.

——, and M. M. Bell, 2007: Rapid intensification, eyewall contraction, and breakdown of Hurricane Charley (2004) near landfall. *Geophys. Res. Lett.,* **34,** L02802, doi:10.1029/2006GL027889.

——, B. J.-D. Jou, P.-L. Chang, and S.-M. Deng, 1999: Tropical cyclone kinematic structure retrieved from single Doppler radar observation. Part I: Interpretation of Doppler velocity patterns and the GBVTD technique. *Mon. Wea. Rev.,* **127,** 2419–2439.

——, ——, ——, and F. D. Marks, 2000: Tropical cyclone kinematic structure retrieved from single Doppler radar observations. Part III: Evolution and structure of Typhoon Alex (1987). *Mon. Wea. Rev.,* **128,** 3982–4001.

——, P. R. Harasti, and M. Bell, 2002: An improved algorithm to resolve circulations of wavenumber two tropical cyclones. Preprints, *25th Conf. on Hurricane and Tropical Meteorology,* San Diego, CA, Amer. Meteor. Soc., 611–612.

——, ——, ——, B. J.-D. Jou, and M.-H. Chang, 2006: Doppler velocity signatures of idealized elliptical vortices. *Terr. Atmos. Oceanic Sci.,* **17,** 429–446.

Marks, F. D., Jr., 2003: State of the science: Radar view of tropical cyclones. *Radar and Atmospheric Science: A Collection of Essays in Honor of David Atlas, Meteor. Monogr.,* No. 30, Amer. Meteor. Soc., 33–74.

——, and R. A. Houze, 1984: Airborne Doppler radar observations in Hurricane Debby. *Bull. Amer. Meteor. Soc.,* **65,** 569–582.

——, and ——, 1987: Inner core structure of Hurricane Alicia from airborne Doppler radar observations. *J. Atmos. Sci.,* **44,** 1296–1317.

——, ——, and J. F. Gamache, 1992: Dual-aircraft investigation of the inner core of Hurricane Norbert. Part I: Kinematic structure. *J. Atmos. Sci.,* **49,** 919–942.

——, P. G. Black, M. T. Montgomery, and R. W. Burpee, 2008: Structure of the eye and eyewall of Hurricane Hugo (1989). *Mon. Wea. Rev.,* **136,** 1237–1259.

Mohr, C. G., L. J. Miller, R. L. Vaughan, and H. W. Frank, 1986: The merger of mesoscale datasets into a common Cartesian format for efficient and systematic analyses. *J. Atmos. Oceanic Technol.,* **3,** 143–161.

Muramatsu, T., 1986a: The structure of polygonal eye of a typhoon. *J. Meteor. Soc. Japan,* **64,** 913–921.

——, 1986b: Trochoidal motion of the eye of Typhoon 8019. *J. Meteor. Soc. Japan,* **64,** 259–272.

Nelder, J. A., and R. Mead, 1965: A simplex method for function minimization. *Comput. J.,* **7,** 308–313.

Nolan, D. S., M. T. Montgomery, and L. Grasso, 2001: The wavenumber-one instability and trochoidal motion of hurricane-like vortices. *J. Atmos. Sci.,* **58,** 3243–3270.

Oye, R., C. Mueller, and S. Smith, 1995: Software for radar translation, visualization, editing and interpolation. Preprints, *27th Conf. on Radar Meteorology*, Vail, CO, Amer. Meteor. Soc., 359–361.

Rappaport, E. N., 1999: Atlantic hurricane season of 1997. *Mon. Wea. Rev.,* **127,** 2012–2026.

Reasor, P. D., M. T. Montgomery, F. D. Marks Jr., and J. F. Gamache, 2000: Low-wavenumber structure and evolution of the hurricane inner core observed by airborne dual-Doppler radar. *Mon. Wea. Rev.,* **128,** 1653–1680.

——, M. D. Eastin, and J. F. Gamache, 2009: Rapidly intensifying Hurricane Guillermo (1997). Part I: Low-wavenumber structure and evolution. *Mon. Wea. Rev.,* **137,** 603–631.

Roux, F., and N. Viltard, 1995: Structure and evolution of Hurricane Claudette on 7 September 1991 from airborne Doppler radar observation. Part I: Kinematics. *Mon. Wea. Rev.,* **123,** 2611–2639.

Willoughby, H. E., 1992: Linear motion of a shallow-water barotropic vortex as an initial-value problem. *J. Atmos. Sci.,* **49,** 2015–2031.

——, and M. B. Chelmow, 1982: Objective determination of hurricane tracks from aircraft observations. *Mon. Wea. Rev.,* **110,** 1298–1305.

Zhao, K., W.-C. Lee, and B. J.-D. Jou, 2008: Single Doppler radar observation of the concentric eyewall in Typhoon Saomei (2006) near landfall. *Geophys. Res. Lett.,* **35,** L07807, doi:10.1029/2007GL032773.